

The Role of Mesons in the Electromagnetic Form Factors of the Nucleon

C. Crawford,¹ T. Akdogan,² R. Alarcon,³ W. Bertozzi,² E. Booth,⁴ T. Botto,² J.R. Calarco,⁵ B. Clasic,² A. DeGrush,² T. W. Donnelly,² K. Dow,² M. Farkhondeh,² R. Fatemi,² O. Filoti,⁵ W. Franklin,² H. Gao,⁶ E. Geis,³ S. Gilad,² D. Hasell,² P. Karpus,⁵ M. Kohl,⁷ H. Kolster,² T. Lee,⁵ E. Lomon,² A. Maschinot,² J. Matthews,² K. McIlhany,⁸ N. Meitanis,² R. Milner,² J. Rapaport,⁹ R. Redwine,² J. Seely,² A. Shinozaki,² A. Sindile,⁵ S. Širca,² E. Six,² T. Smith,¹⁰ B. Tonguc,³ C. Tschalaer,² E. Tsentalovich,² W. Turchinets,² Y. Xiao,² W. Xu,⁶ C. Zhang,² Z. Zhou,² V. Ziskin,² and T. Zwart²

¹*University of Kentucky, Lexington, KY 40504*

²*Physics Department and/or Laboratory for Nuclear Science and/or
Center for Theoretical Physics and/or Bates Linear Accelerator Center,
Massachusetts Institute of Technology, Cambridge, MA 02139*

³*Arizona State University, Tempe, AZ 85287*

⁴*Boston University, Boston, MA 02215*

⁵*University of New Hampshire, Durham, NH 03824*

⁶*Duke University, Durham, NC 27708-0305*

⁷*Hampton University, Hampton, VA 23664*

⁸*United States Naval Academy, Annapolis, MD 21402*

⁹*Ohio University, Athens, OH 45701*

¹⁰*Dartmouth College, Hanover, NH 03755*

(Dated: November 6, 2018)

Abstract

The roles played by mesons in the electromagnetic form factors of the nucleon are explored using as a basis a model containing vector mesons with coupling to the continuum together with the asymptotic Q^2 behavior of perturbative QCD. Specifically, the vector dominance model (GKex) developed by Lomon is employed, as it is known to be very successful in representing the existing high-quality data published to date. An analysis is made of the experimental uncertainties present when the differences between the GKex model and the data are expanded in orthonormal basis functions. A main motivation for the present study is to provide insight into how the various ingredients in this model yield the measured behavior, including discussions of when dipole form factors are to be expected or not, of which mesons are the major contributors, for instance, at low- Q^2 or large distances, and of what effects are predicted from coupling to the continuum. Such insights are first discussed in momentum space, followed by an analysis of how different and potentially useful information emerges when both the experimental and theoretical electric form factors are Fourier transformed to coordinate space. While these Fourier transforms should not be interpreted as “charge distributions”, nevertheless the roles played by the various mesons, especially which are dominant at large or small distance scales, can be explored via such experiment–theory comparisons.

PACS numbers: 12.40.Vv, 13.40.Gp, 14.20.Dh, 25.30.Bf

I. INTRODUCTION

Whether one uses hadronic language involving some set of baryons and mesons or QCD language with quarks and gluons, the nucleon is not a point Dirac particle, but has spatial extension. Its properties may be described, in a large part, in terms of a set of elastic electric and magnetic form factors, G_E^p , G_E^n , G_M^p , and G_M^n arising in EM elastic electron scattering from protons and neutrons, G_A arising when the weak interaction plays a role, together with G_E^s and G_M^s , the strangeness form factors which may play a role in parity-violating elastic electron scattering. In this paper we focus on the first four, the electric and magnetic form factors of the proton and neutron. Clearly having a detailed understanding of all of the form factors of the nucleon constitutes a major goal in physics. These are central to our understanding of strongly-coupled QCD and form the building blocks for much of what is done in exploring the electroweak structure of nuclei.

In experimental studies the electromagnetic form factors of the proton have traditionally been extracted using the Rosenbluth equation for elastic electron scattering from hydrogen, *i.e.* with no polarization information (no polarized electrons, no polarized hydrogen target, no measurement of the recoiling proton polarization). The Rosenbluth differential cross section may be written as:

$$\frac{d\sigma_0}{d\Omega}(E_e, \theta_e) = \frac{\sigma_{Mott}(E_e, \theta_e)}{(1 + \tau)\varepsilon} [\varepsilon(G_E^p(\tau))^2 + \tau(G_M^p(\tau))^2] \quad (1)$$

where $\tau \equiv |Q^2|/4m_p^2$ is the dimensionless 4-momentum transfer and

$$\varepsilon \equiv [1 + 2(1 + \tau) \tan^2 \theta_e/2]^{-1} \quad (2)$$

is the so-called virtual photon polarization, governing the balance between longitudinal and transverse responses. The factor σ_{Mott} is the Mott cross section [1], *i.e.* the cross section for scattering from structureless fermions. In deriving Eq. (1) it has been assumed that the one-photon-exchange approximation is valid. In principle, by varying the electron scattering angle θ_e at fixed τ , one can separate G_E^p from G_M^p . At low Q^2 this is the usual procedure; however, at high Q^2 typically the term involving the magnetic form factor dominates, with the term involving the electric form factor contributing only at the few percent level.

Effects beyond the one-photon-exchange approximation are thought to play a significant role [2–4] and thereby modify Eq. (1) from its standard Rosenbluth form. At low Q^2 the

present understanding is that such contributions provide relatively small corrections, and thus Eq. (1) is a reasonably good approximation. In contrast, at high Q^2 this is not believed to be the case, making relatively large corrections necessary before G_E^p can be extracted using the Rosenbluth cross section. A simple estimate can help to make this clear. Defining the ratio

$$\xi_p \equiv \frac{G_E^p}{\sqrt{\tau}G_M^p} = \frac{R_p}{\mu_p\sqrt{\tau}} \quad (3)$$

where $R_p \equiv \mu_p G_E^p/G_M^p$ (see discussions in Sect. III), the Rosenbluth cross section in Eq. (1) is seen to be proportional to $1 + \varepsilon\xi_p^2$. Using either the model to be discussed in the next section or the data in the following section, one finds that at $Q^2 = 1(5)$ (GeV/c)² one has $\xi_p \sim 0.6(0.1)$. Accordingly, in the latter case the second term (the one containing $(G_E^p)^2$) is only about 1% of the first term, namely, about α ; as a consequence it is not surprising that higher-order QED corrections play a role. This issue will be definitively resolved when new measurements are made using both electrons and positrons to exploit the sign change that occurs in the interference between one and two-photon exchange contributions when the lepton sign is reversed. Experiments are planned or in progress to address these issues at JLab, Novosibirsk and DESY(OLYMPUS).

In recent decades new approaches have been used to separate G_E^p from G_M^p , namely by using polarized electrons and either polarized hydrogen targets, $^1\vec{H}(\vec{e}, e'p)$, or by measuring the recoil polarization of the proton in the final state after the elastic scattering, $^1H(\vec{e}, e'\vec{p})$. For instance, for the polarized electron/polarized target case one has

$$\frac{d\sigma}{d\Omega}(E_e, \theta_e; \theta^*, \phi^*) = \frac{d\sigma_0}{d\Omega}(E_e, \theta_e) \left[1 + p_e \vec{p}_T \cdot \vec{A}(\tau, \varepsilon; \theta^*, \phi^*) \right] \quad (4)$$

where p_e is the longitudinal electron polarization, \vec{p}_T is a vector pointing in the direction characterized by the angles (θ^*, ϕ^*) in a coordinate system with z-axis along the virtual photon direction and with the normal to the electron scattering plane lying along the y-axis (see [5]). The polarization information is contained in the product

$$\vec{p}_T \cdot \vec{A}(\tau, \varepsilon; \theta^*, \phi^*) \sim \sqrt{2\varepsilon}G_E^p(\tau)G_M^p(\tau) \sin\theta^* \cos\phi^* + \sqrt{\tau(1+\varepsilon)}(G_M^p(\tau))^2 \cos\theta^* \quad (5)$$

and clearly by flipping the electron's helicity and/or the target's spin and choosing the target polarization to lie in at least two different directions it is possible, at least in principle, to separate the interference $G_E^p G_M^p$ from the term having $(G_M^p)^2$. Experimentally it is

clearly advantageous to form a ratio of the result given above for two choices of polarization directions, say (θ_1^*, ϕ_1^*) and (θ_2^*, ϕ_2^*) :

$$\frac{\vec{p}_T \cdot \vec{A}(\tau, \varepsilon; \theta_1^*, \phi_1^*)}{\vec{p}_T \cdot \vec{A}(\tau, \varepsilon; \theta_2^*, \phi_2^*)} = \frac{\sqrt{2\varepsilon}G_E^p(\tau)G_M^p(\tau) \sin \theta_1^* \cos \phi_1^* + \sqrt{\tau(1+\varepsilon)}(G_M^p(\tau))^2 \cos \theta_1^*}{\sqrt{2\varepsilon}G_E^p(\tau)G_M^p(\tau) \sin \theta_2^* \cos \phi_2^* + \sqrt{\tau(1+\varepsilon)}(G_M^p(\tau))^2 \cos \theta_2^*} \quad (6)$$

$$= \frac{\frac{\sqrt{2\varepsilon}}{\sqrt{\tau(1+\varepsilon)}} \frac{G_E^p(\tau)}{G_M^p(\tau)} \sin \theta_1^* \cos \phi_1^* + \cos \theta_1^*}{\frac{\sqrt{2\varepsilon}}{\sqrt{\tau(1+\varepsilon)}} \frac{G_E^p(\tau)}{G_M^p(\tau)} \sin \theta_2^* \cos \phi_2^* + \cos \theta_2^*} \quad (7)$$

When, as is typically done, the choice is made to employ parallel (\parallel : $\theta_2^* = 0$) and perpendicular (\perp : $\theta_1^* = \pi/2$, $\phi_1^* = 0$) kinematics, this provides a way to determine the ratio of the form factors:

$$\sqrt{\frac{\tau(1+\varepsilon)}{2\varepsilon}} \cdot \frac{A_\perp}{A_\parallel} = \frac{G_E^p(\tau)}{G_M^p(\tau)} \quad (8)$$

Similar expressions occur when measuring the recoil polarization (see, for example, [5, 6]).

Analogous studies whose goal is to extract the form factors of the neutron must generally be undertaken by electron scattering from few-body nuclei. In particular, inclusive quasi-elastic scattering of polarized electrons from polarized ^3He , namely, $^3\vec{H}e(\vec{e}, e')X$, and semi-inclusive quasi-elastic scattering of polarized electrons from either polarized deuterons or ^3He , namely, $^2\vec{H}(\vec{e}, e'n)p$ and $^3\vec{H}e(\vec{e}, e'n)X$, respectively, or with polarization transfer to final-state neutrons, $^2H(\vec{e}, e'\vec{n})p$, have all been used to provide effectively elastic electron scattering from neutrons, *i.e.*, $\vec{e} + \vec{n} \rightarrow e' + n$ and $\vec{e} + n \rightarrow e' + \vec{n}$. Naturally, in these cases some corrections for nuclear physics effects must be made. The separation of the neutron electromagnetic form factors benefits in two ways from the use of polarized data. Not only is the sensitivity to two-photon corrections decreased, but also some of the nuclear model dependence cancels in the form factor ratio.

Note that, since the form factors occur as interferences in Eq. (5) and therefore one is not at high Q^2 comparing a very small contribution (G_E^2) with a very large contribution (G_M^2) as occurs in the Rosenbluth cross section, it is believed that one is not as sensitive to higher-order corrections beyond the one-photon-exchange approximation. This is borne out in modeling of the two-photon effects [2–4] which indicate that the Rosenbluth cross section is problematical in this regard, as mentioned above, but that these corrections are relatively much less important for the extraction of the form factor ratio using polarization observables and that, accordingly, using polarization degrees of freedom in elastic ep scattering can provide a clean separation of the form factors. Again, to make this clear, let us use the

simple estimate as above. The result in Eq. (5) is proportional to

$$\vec{p}_T \cdot \vec{A}(\tau, \varepsilon; \theta^*, \phi^*) \sim \sqrt{\frac{2\varepsilon}{1+\varepsilon}} \xi_p \sin \theta^* \cos \phi^* + \cos \theta^* \quad (9)$$

and thus, even at $Q^2 = 5 \text{ (GeV/c)}^2$ where ξ_p was seen to be about 0.1, the first term (for ε not too small) is typically 10% of the second and higher-order $\mathcal{O}(\alpha)$ QED corrections probably make less of an impact on the extraction of the form factor ratio.

On the theoretical side, exact *ab initio* QCD calculations of $G_{E,M}^{p,n}$ using lattice techniques will eventually be possible. However, despite the fact that very encouraging results have been obtained in recent work [7], a fully quantitative understanding of the entire set of form factors is lacking at present. Given this, alternative approaches are typically taken. For example, light-front methods, quark descriptions and chiral invariance have been employed by Miller to obtain qualitative relations and semi-quantitative descriptions of various aspects of the form factors in both momentum and configuration space [8–15].

In the present work we draw upon results from form factor models which use as hadronic building blocks vector mesons together with coupling to the $\pi\pi$, $\pi\pi\pi$, and $K\bar{K}$ continua as given by dispersion relation calculations — the so-called Vector Meson Dominance plus Dispersion Relation based models (VMD+DR) [8, 16–23]. The most recent versions of these models have been quite successful in representing the momentum-space content in the form factors, *i.e.*, the behaviors of the form factors as functions of 4-momentum transfer squared, especially the models which also incorporate ingredients that provide the correct asymptotic behavior as $Q^2 \rightarrow \infty$ (see Sect. II). For instance, as discussed in more detail later, one sees that, in some cases, cancellations of various vector meson contributions can lead to a dipole-like Q^2 -dependence, which is in good agreement with the nucleon’s magnetic form factors for $Q^2 < 5 \text{ (GeV/c)}^2$. The proton’s electric form factor is known to fall faster than dipole and, in fact, even the earliest VMD+DR models [16, 17] showed this behavior although the available data did not. At low Q^2 the neutron’s electric form factor has a different form from the proton’s, since the net charge in the neutron is zero; again the polarization data and VMD+DR approaches yield a Q^2 -dependence for G_E^n which is only in rough accord over the current experimental range with the commonly used dipole type approximation, namely, the Galster form [24]. In the most recent fits, such as in [23, 25] where the high- Q^2 behavior predicted by perturbative QCD is enforced, all four of the nucleon’s electromagnetic form factors are very well represented, showing the experimentally indicated deviations from the

dipole or Galster forms. This will be discussed in more detail in Sect. II. Additionally, a few remarks will be made there concerning the differences between the VMD+DR approach with hadronic form factors used here for comparison with data [23] and a version without such form factors where instead one adds effective vector mesons [25].

In addition to discussing the form factors in Sect. II, both the measured quantities and the VMD+DR modeling, *i.e.* the momentum-space content, we also discuss results in coordinate space (see Sect. V) with the goal being to obtain additional insights both into the various representations of the data (p versus n, G_E versus G_M , isoscalar versus isovector, u-quark versus d-quark) and into the roles being played by the various ingredients in the VMD+DR approach (the different vector mesons, the role of the coupling to the continuum, the nature of terms that yield the asymptotic behavior).

The paper is organized in the following way: following this introduction, in Sect. II the reference model is discussed in some detail. The basic formalism is summarized, together with a brief discussion of the data-fitting procedure. Results from the reference model, denoted GKex, are presented in Sect. III, followed by a brief discussion where the GKex reference model is compared with another recent model denoted BHM. In Sec IV the reference model is used to attempt to gain some insights into how the various contributions work with or against each other to produce the observed form factors. The Breit-frame Fourier transforms of $G_E^{p,n}$ are discussed in Sect. V, beginning with some general caveats on the meaning and relevance of representing results in coordinate space and proceeding in Sect. VA to discuss the procedures used to obtain the Fourier transfers starting with data in momentum space and to estimate the uncertainties on the resulting coordinate-space representations. In Sect. VB the resulting Breit-frame densities are presented and discussed, and alternative representations are given (isoscalar/isovector, u-quark/d-quark). Again in this section the reference model is employed to help in understanding how the various ingredients enter in producing the Breit-frame Fourier transforms. Finally, in Sect. VI conclusions resulting from this study are summarized.

II. THE GKEX MODEL

Given the brief introductory discussions in Sect. I to place the general problem in context, let us now summarize the ingredients in the basic model employed in the present work. We

consider only the VMD+DR approach, as this provides a reasonably successful representation of the nucleon's electromagnetic form factors. We start by summarizing some of the basic formulas needed in the discussions to follow. In particular, the electromagnetic form factors of a nucleon are defined via the expression for the electromagnetic current matrix element

$$\langle N(p') | J_\mu | N(p) \rangle = \bar{u}(p') \left[\gamma_\mu F_1^N(Q^2) + \frac{i}{2m_N} \sigma_{\mu\nu} q^\nu F_2^N(Q^2) \right] u(p), \quad (10)$$

where $q_\mu \equiv p_\mu - p'_\mu$, $Q^2 \equiv -q_\mu^2 \geq 0$ (in the space-like regime) is the square of the invariant momentum transfer, N is the neutron, n , or proton, p , and $F_1^N(Q^2)$ and $F_2^N(Q^2)$ are respectively the Dirac and Pauli form factors, normalized at $Q^2 = 0$: $F_1^p(0) = 1$, $F_1^n(0) = 0$, $F_2^p(0) = \kappa_p$ and $F_2^n(0) = \kappa_n$ where κ_p and κ_n are the anomalous magnetic moments for the proton and neutron, respectively. The Sachs form factors, most directly obtained from experiment, are then

$$G_E^N(Q^2) = F_1^N(Q^2) - \tau F_2^N(Q^2) \quad (11)$$

$$G_M^N(Q^2) = F_1^N(Q^2) + F_2^N(Q^2) \quad (12)$$

and the combinations measured by the polarization experiments are

$$R_N \equiv G_E^N / (G_M^N / \mu_N). \quad (13)$$

The isoscalar and isovector form factors are, respectively

$$F_{1,2}^{(0)}(Q^2) \equiv F_{1,2}^p(Q^2) + F_{1,2}^n(Q^2) \quad (14)$$

$$F_{1,2}^{(1)}(Q^2) \equiv F_{1,2}^p(Q^2) - F_{1,2}^n(Q^2). \quad (15)$$

Electrons couple through photons to the electromagnetic currents provided by the hadron and quark distributions within the nucleons, yielding the form factors introduced above. Because the photon is a vector particle, at any parity-conserving vertex where it couples with hadrons it must connect to these hadrons with unit total angular momentum and negative parity. The photon does not conserve isospin and so these systems of hadrons may be isoscalar or isovector. The simplest such vertex connects the photon to a single vector meson (ρ , ω , ϕ , ...). It can also couple to systems of two or three pions or $K\bar{K}$ in a 1^- state, which in turn may couple to a ρ , ω or ϕ -type meson. Since the latter are resonances of the multi-meson systems, the strength of the interaction is largest close to

the masses of the vector mesons. In leading order this is the VMD limit of the photon-hadron interaction [26] which will be seen to give a good representation of the data over most of the present range of momentum transfers (see below). However, small but significant corrections can be expected from multi-pion correlations in the continuum, such as those that give the ρ meson its width. These contributions can be calculated using dispersion relations with input from meson-meson scattering. At sufficiently high momentum transfers, as perturbative Quantum Chromodynamics (pQCD) becomes a better approximation than effective hadrons, photons coupling to quarks provides a better description and the models must asymptotically have a pQCD behavior. This transition is handled in various ways by the models, as discussed later.

The earliest reasonable fit to the available nucleon form factor data was a VMD model [16] of Iachello, Jackson and Lande with ρ , ω and ϕ vector meson poles. They incorporated a single meson/nuclear vertex form factor for all terms, using various forms that cut-off at high momentum transfer (but none decreased as rapidly as pQCD). The width of the rho-meson was included by modifying the pole term with a form suggested by Frazer and Fulco [27]. A more recent paper by Bijker and Iachello [28] adds an asymptotic term to the Pauli-isovector current and modifies the hadronic form factor to include the asymptotic logarithmic Q dependence. After refitting parameters to a larger set of data, the neutron form factors are substantially improved at the expense of a small worsening in the fit to the proton form factors compared with earlier fit [16].

Shortly after [16] Höhler and collaborators [17] used dispersion relations to obtain the contribution of the $\pi\pi$ continuum giving the ρ meson its width, which they fitted with a simple function of the mass (Eq. (4.2) of that reference). The ω and ϕ mesons and several phenomenological vector mesons were represented by simple poles. They did not introduce form factors at the strong vertices. Instead the phenomenological constants (pole masses and residues) were restricted by conditions of super-convergent behavior at asymptotic momentum transfers in addition to being optimized to fit the data. This required the addition of unknown vector meson pole terms.

Recently Meissner and collaborators [25, 29] have extended the Höhler type model by considering, in addition to the $\pi\pi$ continuum, the $K\bar{K}$ and $\rho\pi$ continua, which they find are adequately represented by simple poles. They also added phenomenological vector meson poles and a broad phenomenological contribution to each isovector form factor at higher

masses. As before, there are no strong vertex form factors and the asymptotic momentum transfer behavior is obtained by requiring a cancellation amongst all of the terms to obtain super-convergence in one fit, and an explicit pQCD behavior in another version.

Gari and Krümpelmann (GK) [30] proposed a model in which VMD at low momentum transfers was replaced by pQCD at high momentum transfers, using differing convergence rates of hadronic and quark form factors. [Also Ref. [18] from earlier.] They obtained a good fit to the data then available using only the ρ , ω and ϕ vector meson poles. The hadronic (quark) form factors are required by the strong renormalization corrections at the vector meson/nucleon (quark) vertices. The ϕ meson-nucleon hadronic form factor has been constructed imposing the Zweig rule required by the $s\bar{s}$ quark structure of that meson. The inclusion of these vertex form factors was crucial in enabling the evolution with momentum transfer to the pQCD behavior without an artificial constraint on the relation between the vector meson pole parameters. As an added indication of the validity of this approach, there was no need for adding several phenomenological vector meson poles at masses in disagreement with available data.

The physical realism of this model was enhanced by Lomon [20, 21, 23] by incorporating the following modifications:

- The width of the ρ meson was included using the dispersion calculation of [25];
- The observed ρ' (1.45 GeV) [20] and ω' (1.419 GeV) [21] vector meson poles were included;
- In [21] and later the quark-nucleon vertex form factor uses the quark-nucleon cut-off, instead of the meson-nucleon cut-off used by GK. Also the vector meson-hadron form factors of GK (model 1) were used as being more consistent with the helicity flip in the Pauli terms. In both cases the logarithmic dependence is determined by Λ_{QCD} , which is fixed near the value determined by high-energy data.

These yielded the so-called GKex (Gari-Krümpelmann extended) models used in the present work. In particular, we employ the model given in [23] as the basis for the present studies. Note that our motivation in the present work is not so much to elaborate the fitting procedures discussed in [21], but to take as given that study and use the model discussed there to gain a deeper understanding of some of the systematics seen in the data. No attempt is

made in the present work to provide new fits to the data after 2005, since the world database is soon to be extended — the form factor representations are frozen, using the one specific contemporary VMD+DR model denoted GKex [23]. Specifically, we wish to obtain better insight into why the $G_M^{p,n}$ form factors are roughly dipole in character, while G_E^p is not, and falls faster than dipole. We shall see that this difference in behavior emerges naturally in the context of the models discussed. Furthermore, the most modern models of the type employed here are actual hybrids containing hadronic ingredients as well as terms which have the correct pQCD behaviors when Q^2 becomes large. Within these models one can ask where the cross-over to this asymptotic behavior occurs.

The GKex model of [21, 23] is summarized in the following. Specifically, the form factors in that model are given by:

$$\begin{aligned}
F_1^{(0)}(Q^2) &\equiv \frac{g_\omega}{f_\omega} f^{em}(m_\omega; Q^2) f_1^{had}(Q^2) \\
&\quad + \frac{g_{\omega'}}{f_{\omega'}} f^{em}(m_{\omega'}; Q^2) f_1^{had}(Q^2) \\
&\quad + \frac{g_\phi}{f_\phi} f^{em}(m_\phi; Q^2) f_1^{had,s}(Q^2) \\
&\quad + \left[1 - \frac{g_\omega}{f_\omega} - \frac{g_{\omega'}}{f_{\omega'}} \right] f_1^{had,pQCD}(Q^2)
\end{aligned} \tag{16}$$

$$\begin{aligned}
F_2^{(0)}(Q^2) &\equiv \kappa_\omega \frac{g_\omega}{f_\omega} f^{em}(m_\omega; Q^2) f_2^{had}(Q^2) \\
&\quad + \kappa_{\omega'} \frac{g_{\omega'}}{f_{\omega'}} f^{em}(m_{\omega'}; Q^2) f_2^{had}(Q^2) \\
&\quad + \kappa_\phi \frac{g_\phi}{f_\phi} f^{em}(m_\phi; Q^2) f_2^{had,s}(Q^2) \\
&\quad + \left[\kappa_s - \kappa_\omega \frac{g_\omega}{f_\omega} - \kappa_{\omega'} \frac{g_{\omega'}}{f_{\omega'}} - \kappa_\phi \frac{g_\phi}{f_\phi} \right] f_2^{had,pQCD}(Q^2)
\end{aligned} \tag{17}$$

$$\begin{aligned}
F_1^{(1)}(Q^2) &\equiv \frac{g_\rho}{f_\rho} f^{em}(m_{\rho_1}; Q^2) f_1^{had}(Q^2) \left[(1 - \alpha_1) + \frac{\alpha_1}{(1 + Q^2/Q_1^2)^2} \right] \\
&\quad + \frac{g_{\rho'}}{f_{\rho'}} f^{em}(m_{\rho'}; Q^2) f_1^{had}(Q^2) \\
&\quad + \left[1 - \frac{g_\rho}{f_\rho} - \frac{g_{\rho'}}{f_{\rho'}} \right] f_1^{had,pQCD}(Q^2)
\end{aligned} \tag{18}$$

$$\begin{aligned}
F_2^{(1)}(Q^2) \equiv & \kappa_\rho \frac{g_\rho}{f_\rho} f^{em}(m_{\rho_2}; Q^2) f_2^{had}(Q^2) \left[(1 - \alpha_2) + \frac{\alpha_2}{(1 + Q^2/Q_2^2)} \right] \\
& + \kappa_{\rho'} \frac{g_{\rho'}}{f_{\rho'}} f^{em}(m_{\rho'}; Q^2) f_2^{had}(Q^2) \\
& + \left[\kappa_v - \kappa_\rho \frac{g_\rho}{f_\rho} - \kappa_{\rho'} \frac{g_{\rho'}}{f_{\rho'}} \right] f_2^{had,pQCD}(Q^2). \tag{19}
\end{aligned}$$

In these expressions the anomalous magnetic moments are $\kappa_s = \kappa_p + \kappa_n$ and $\kappa_v = \kappa_p - \kappa_n$, and the κ_x are the analogous quantities associated with the vector mesons $x = \rho, \rho', \omega, \omega'$ and ϕ . The pole corresponding to a vector meson of mass m_x yields the monopole form

$$f^{em}(m_x; Q^2) \equiv \left[\frac{m_x^2}{m_x^2 + Q^2} \right] \quad x = \rho, \rho', \omega, \omega', \phi \tag{20}$$

and the coupling constant of each pole is g_x/f_x , $x = \rho, \rho', \omega, \omega'$ and ϕ , where g_x is the coupling of meson to the nucleon and f_x is given by the coupling of the meson to the photon. The value of f_x is experimentally determined from the meson decay to e^+e^- .

For completeness we briefly summarize the procedures used in [20, 21, 23] to determine the model parameters. Specifically, the 2001 version of the GKex model, which did not include the ω' meson, was fitted to all of the unpolarized, Rosenbluth-separated cross section data, and included the then-available R_p polarization data, although in the absence of R_n data. The 2002 GKex model includes the then-available polarization R_p and R_n data, some of which was not final. The present 2005 GKex model — the one used as a basis for the present study — differs from the 2002 version only due to the substitution of the final polarization data, inclusion of the few new R_n and G_M^n points, and the exclusion of the higher Q^2 $G_E^{p,n}$ data from the Rosenbluth separation of differential cross section data. For completeness we list the parameters obtained using the last model [23]. Given the fact that new data will soon be available, no re-fitting has been done for the present study, although it is anticipated that this will be performed in the near future. The masses of the known vector mesons are fixed: $m_\rho = 0.776$ GeV, $m_\omega = 0.784$ GeV, $m_{\rho'} = 1.45$ GeV, $m_{\omega'} = 1.419$ GeV and $m_\phi = 1.019$ GeV. The ratios g/f are as follows: $g_\rho/f_\rho = 0.5596$, $g_\omega/f_\omega = 0.7021$, $g_{\rho'}/f_{\rho'} = 0.0072089$, $g_{\omega'}/f_{\omega'} = 0.164$ and $g_\phi/f_\phi = -0.1711$. The vector mesons' anomalous magnetic moments are $\kappa_\rho = 5.51564$, $\kappa_\omega = 0.4027$, $\kappa_{\rho'} = 12.0$, $\kappa_{\omega'} = -2.973$, $\kappa_\phi = 0.01$ and one finds that $\mu_\phi = 0.2$.

Defining

$$\tilde{Q}^2 \equiv Q^2 \frac{\ln [(\Lambda_D^2 + Q^2) / \Lambda_{QCD}^2]}{\ln [\Lambda_D^2 / \Lambda_{QCD}^2]}, \tag{21}$$

with $\Lambda_D = 1.181$ GeV and $\Lambda_{QCD} = 0.150$ GeV (fixed), thereby incorporating the logarithmic momentum transfer behavior of pQCD, the hadronic vector-meson to nucleon form factors for those vector mesons dominantly consisting of non-strange quarks (ρ , ω , ρ' and ω') are given by

$$f_1^{had}(Q^2) \equiv f(\Lambda_1; \tilde{Q}^2)f(\Lambda_2; \tilde{Q}^2) \quad (22)$$

$$f_2^{had}(Q^2) \equiv f(\Lambda_1; \tilde{Q}^2)f(\Lambda_2; \tilde{Q}^2)^2, \quad (23)$$

where

$$f(\Lambda_i; \tilde{Q}^2) \equiv \left[\frac{\Lambda_i^2}{\Lambda_i^2 + \tilde{Q}^2} \right], \quad (24)$$

i.e. functionally the same (monopole) expression as Eq. (20), now with $m_x \rightarrow \Lambda_i$ and $Q^2 \rightarrow \tilde{Q}^2$. From the fit one has $\Lambda_1 = 0.93088$ GeV and $\Lambda_2 = 2.6115$ GeV.¹ The spin-flip nature of the Pauli term in the current is the origin of the extra power of $f(\Lambda_2; \tilde{Q}^2)$ in Eq. (23).

For the ϕ meson, which is dominantly composed of strange quarks, the hadronic form factors are given by

$$f_1^{had,s}(Q^2) \equiv f_1^{had}(Q^2) \left[\frac{Q^2}{\Lambda_1^2 + Q^2} \right]^{3/2} \quad (25)$$

$$f_2^{had,s}(Q^2) \equiv f_2^{had}(Q^2) \left[\frac{\mu_\phi^2 + Q^2}{\mu_\phi^2} \frac{\Lambda_1^2}{\Lambda_1^2 + Q^2} \right]^{3/2}. \quad (26)$$

The form factor $f_1^{had,s}$ vanishes at $Q^2 = 0$, and it and $f_2^{had,s}$ decrease more rapidly at large Q^2 than the other meson form factors. This conforms to the Zweig rule imposed by the $s\bar{s}$ structure of the ϕ meson [31]. Only 10 of the 12 parameters listed above are independent, as κ_ϕ/μ_ϕ and $\kappa_{\rho'}g_{\rho'}/f_{\rho'}$ are constrained to be very close to 0.05 and 0.08, respectively. The fit has little sensitivity to Λ_{QCD} , which is fixed at 0.150 in its experimental range.

All of the terms but two in the above isoscalar and isovector form factors are of the pole form representing a vector meson exchange. However, the first term in each of the isovector form factors is an approximate analytic form for a ρ meson with a width derived from a dispersion integral of the $\pi\pi$ continuum. For later discussions, we have written

¹ The constants used in the GKex model are given here to high precision not because they are so well known, but because they will allow others to program the formulas in this section and check their results against the results found in the present study.

these expressions using parameters α_1 (α_2) for the $F_1^{(1)}$ ($F_2^{(1)}$) expressions, respectively, where $\alpha_1 = 0.0781808$ and $\alpha_2 = 0.0632907$ when the widths are included, with $\alpha_i = 0$, $i = 1, 2$ when the effect from coupling to the continuum is ignored. In addition, when the contributions from the continuum are included, the effective ρ mass is shifted down slightly from the physical mass: $m_{\rho_i} = m_\rho - \delta_i$ with $\delta_1 = 34.65$ MeV and $\delta_2 = 43.74$ MeV. When the ρ contributions are taken to occur only at the pole, of course these shifts are also neglected and the physical mass used in the expressions above. The momentum cutoffs in the terms that occur when the width is included are $Q_1^2 = 0.3176$ (GeV/c)² and $Q_2^2 = 0.1422$ (GeV/c)². All of these constants are determined by a dispersion calculation and we use the results obtained by [29]. Note that turning off the width and using only the ρ -pole form is not fully consistent: one should refit the data with the $\alpha_i = 0$ to do this correctly. However, for our present purposes simply turning the width off gives us some indication of where one might expect the coupling to the $\pi\pi$ continuum to play a role, either in momentum space or in coordinate space.

For the asymptotic terms, the form factors due to the coupling of the mesons to the nucleons at the quark level are given by

$$f_1^{had,pQCD}(Q^2) \equiv f(\Lambda_D; \tilde{Q}^2)f(\Lambda_2; \tilde{Q}^2) \quad (27)$$

$$f_2^{had,pQCD}(Q^2) \equiv f(\Lambda_D; \tilde{Q}^2)f(\Lambda_2; \tilde{Q}^2)^2. \quad (28)$$

The coefficients of these terms impose the constraints at $Q^2 = 0$,

$$\begin{aligned} F_1^{(0)}(0) &= F_1^{(1)}(0) = 1 \\ F_2^{(0)}(0) &= \kappa_s \quad F_2^{(1)}(0) = \kappa_v, \end{aligned} \quad (29)$$

and when $Q^2 \rightarrow \infty$ have the asymptotic forms

$$\begin{aligned} F_1^{(0,1)} &\rightarrow \frac{1}{Q^2 \ln(Q^2/\Lambda_{QCD}^2)} \\ F_2^{(0,1)} &\rightarrow \frac{1}{Q^4 \ln(Q^2/\Lambda_{QCD}^2)} \end{aligned} \quad (30)$$

as required by pQCD.

The GKex model employed in the present study is the one of [23] with the parameters fitted to a large data set, for which the low- Q^2 BLAST data were not yet available. Included in the data set were G_M^p and G_M^n from Rosenbluth separations of unpolarized cross sections,

and R_p and R_n obtained from polarization measurements, over the whole experimental energy range. The G_E^p and G_E^n results obtained by Rosenbluth separation of the unpolarized cross sections were only included at lower Q^2 where they are more than a few percent of the magnetic cross section, and therefore not too sensitive to the two-photon contributions discussed in Sect. I. At higher Q^2 the $G_E^{p,n}$ from the Rosenbluth separations are systematically larger than those obtained by multiplying the polarization observables, $R_{p,n}$ by the $G_M^{p,n}$ obtained from the unpolarized cross sections. A recent higher accuracy measurement [32] of the unpolarized cross section confirms this result.

In detail, the data from Refs. 7–14, and 16–36 cited in [20] were used, with the omission of the G_E^p values for $Q^2 \geq 1.75$ (GeV/c)² of Ref. 7 and the G_E^n values for $Q^2 \geq 0.779$ (GeV/c)² of Refs 9, 17, and 18 there. Reference [23] used the R_p values of Ref. 5, the R_n values of Refs. 4 and 6 and the recent G_M^n data of Ref. 7. It should be emphasized that the form factor data sets were all fit simultaneously. Another datum used is the slope $dG_E^n/dQ^2(Q^2 = 0) = 0.0199 \pm 0.0003$ fm², as determined by thermal neutron scattering [33, 34]. Although this is the most accurate G_E^n information, it is often not considered in model fitting.

III. RESULTS IN MOMENTUM SPACE AND COMPARISONS WITH DATA

Fig. 1 shows R_p as represented by the GKex model [23] (fitted to the data listed at the end of Sect. II) together with the polarization data [35–38]. The R_p data used in the fit were the polarization measurements of [35, 36] and (not shown) the ratio extracted from a Rosenbluth separation [40], while the results presented in [37, 38] were not used in the fit. The model fits the polarization data well while not conforming to the results obtained from Rosenbluth separations. Moreover, as shown, this fit predicted the new BLAST low momentum transfer results [37, 38] well and is in excellent agreement with the very recent results at higher Q^2 from JLab [41]. The deviation from unity is substantial for $Q^2 > 0.8$ (GeV/c)²; indeed, as stated in the previous section, this has always been a feature of the VMD class of models in that from their inception they have typically led to a fall-off with Q^2 of G_E^p compared with the dipole form factor.

Fig. 2 displays the model result for $G_M^p/\mu_p G_D$, where G_D is the standard dipole form. The model was fitted to all the Rosenbluth determinations of G_M^p data [40, 42–48]. In addition the data from [31] and the more recent precision data [32] is shown. The momentum transfer

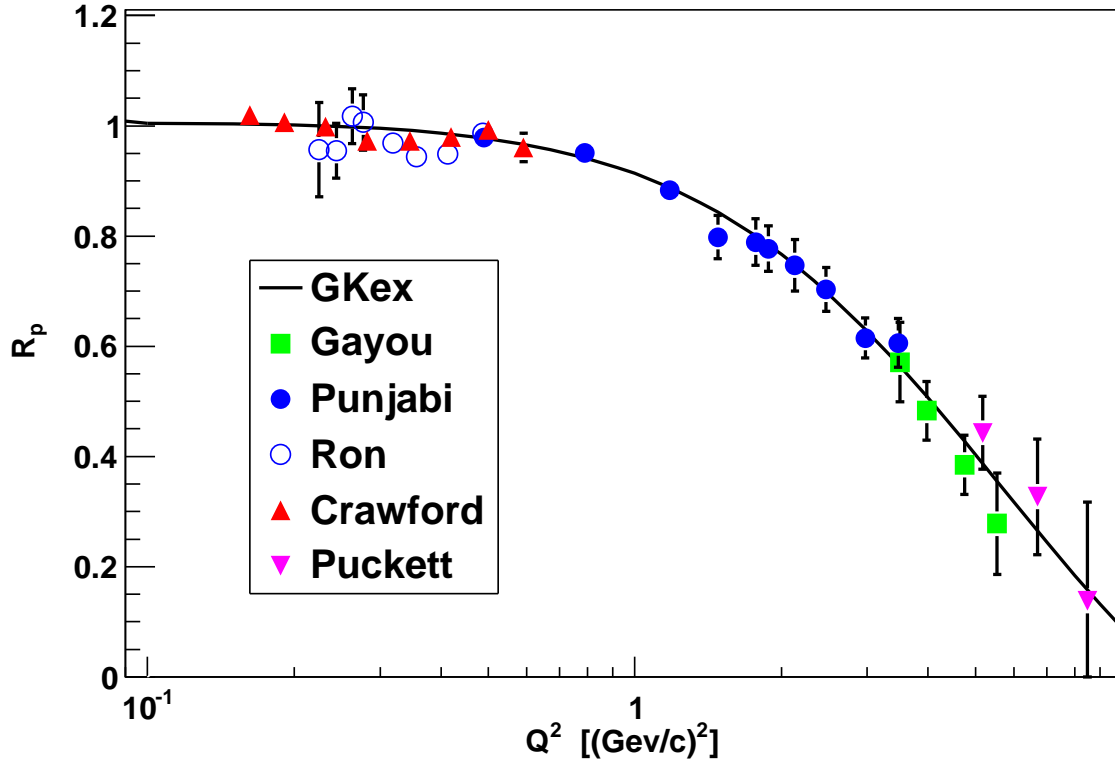


FIG. 1: Form factor ratio R_p showing the GKex universal fit [23] together with the fitted data (Gayou [35], Punjabi [36], and Ron [37]; see the end of Sect: II) and recent measurements from BLAST (Crawford [38]) and JLab (Puckett [39]). In color online.

range is greater than for the other form factors. The ratio is relatively close to unity until $Q^2 \approx 1$ when it increases before decreasing rapidly for $Q^2 > 7$ (GeV/c)².

Fig. 3 shows the model results for G_E^p/G_D . The model was fitted to the low- Q^2 G_E^p differential cross section data of [42–44, 49]. For the reasons given above (small contribution to the unpolarized cross section and 2-photon corrections) the higher- Q^2 data displayed [32, 47, 48] were not included in the fitting procedure. Also shown are data [31] and the G_E^p values given by the polarization values of R_p [35, 36] multiplied by the model G_M^p/μ_p . Above 1.8 (GeV/c)² the model fits the polarization values, but not those obtained from Rosenbluth separations.

The extraction of the neutron form factors from quasi-elastic electron-deuteron or electron-³He scattering, with their dependence on the nuclear wave function and hadronic final-state interactions, leads to greater uncertainties and a more restricted momentum trans-

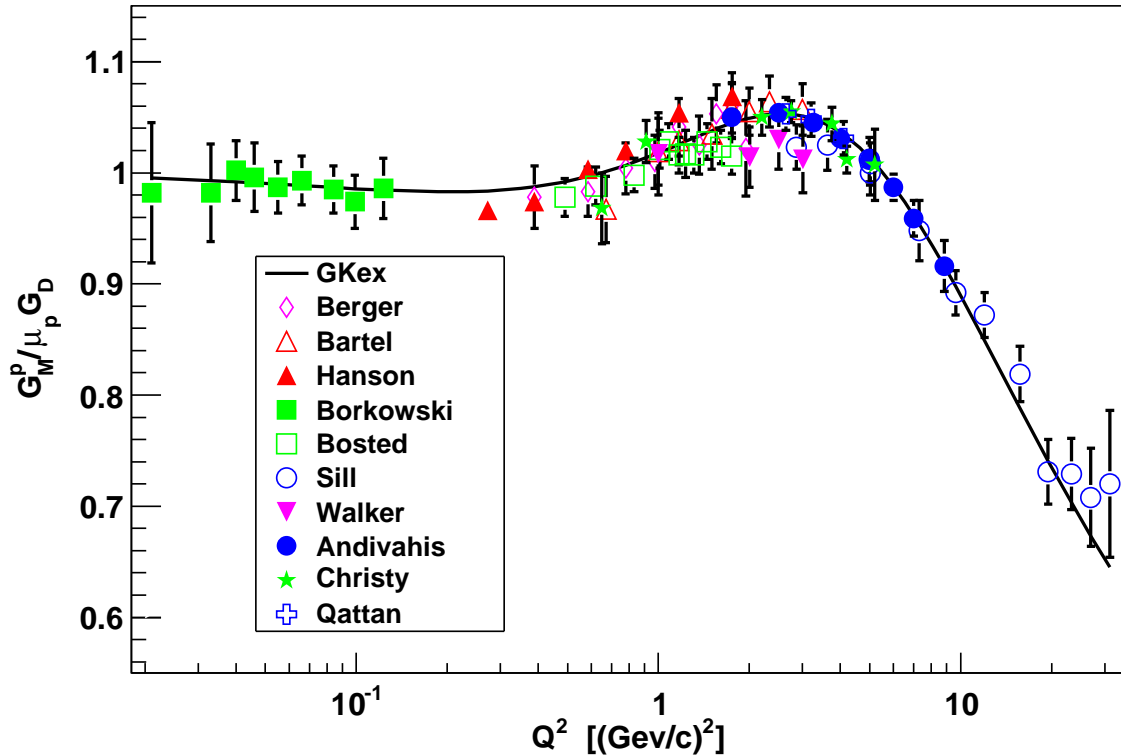


FIG. 2: The ratio $G_M^p/\mu_p G_D$ with the GKex universal fit [23] and the fitted data (Berger [42], Bartel [40], Hanson [43], Borkowski [44], Bosted [45], Sill [46], Walker [47], and Andivahis [48]; see the end of Sect: II). In addition the data from Christy [31] and the more recent precision data Qattan [32] are shown. In color online.

fer range than for the proton form factor. There is also some evidence at the highest available momentum transfers of the deviation from the dipole form for the magnetic form factor, and from the modified dipole (Galster) form for the electric-to-magnetic ratio.

Fig. 4 shows R_n given by the GKex model [23]. In that model only the polarization data of [50, 51] were fitted, but not the more recent low- Q^2 BLAST data [52] nor the preliminary higher- Q^2 JLab data [53]. Nevertheless, the 2005 fit agrees very well with the BLAST results and with the preliminary data (not shown). The Galster form (dashed curve) is also shown, the slope of which at $Q^2 = 0$ is known to be larger than that obtained from cold neutron scattering. As seen in the figure this results in the Galster curve being above the BLAST data and the model curve up to 0.4 (GeV/c)^2 . Above that momentum transfer the Galster expression drops below the data and the model curve.

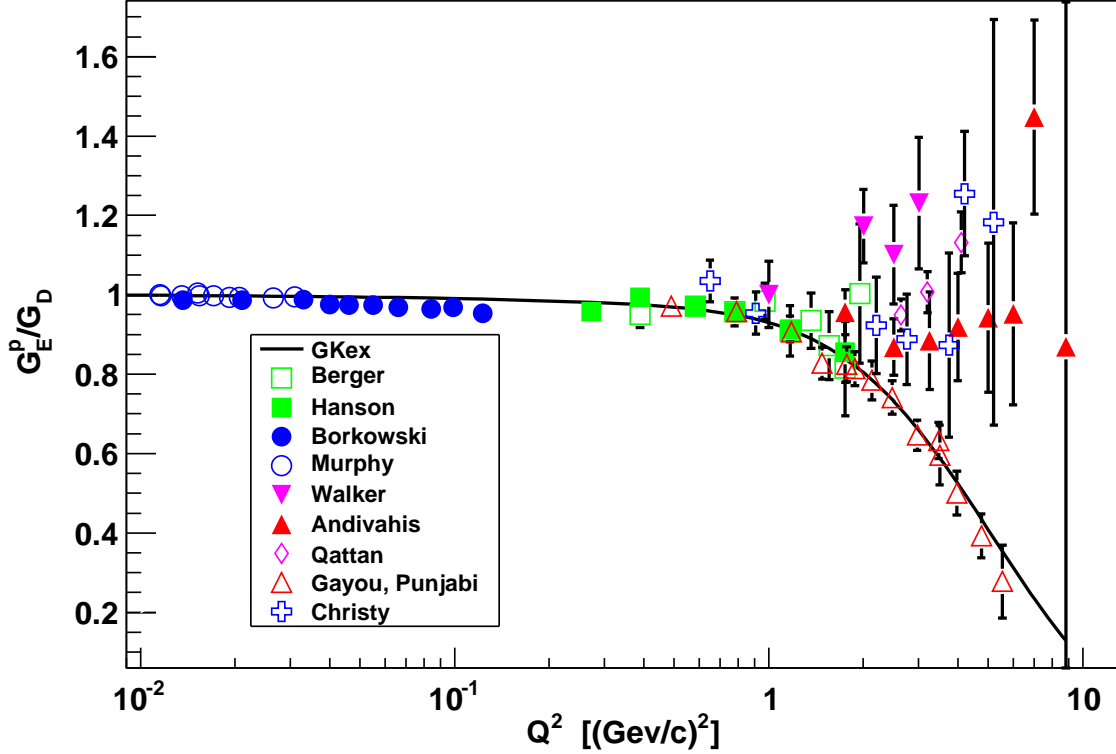


FIG. 3: The ratio G_E^p/G_D with the GKex universal fit [23]. Because the higher momentum-transfer values obtained from the Rosenbluth separation are not considered reliable, only the lower momentum-transfer values from Rosenbluth separation (Berger [42], Hanson [43], Borkowski [44], and Murphy [49]) were included in the fitting. However, the higher momentum-transfer values (Walker [47], Andivahis [48], and Qattan [32]; see the end of Sect: II) are also plotted. The fitted R_p data of Gayou [35] and Punjabi [36] were translated to G_E^p by multiplying by the GKex G_M^p/μ_p . Data from Christy [31] is also shown. In color online.

All of the G_M^n data [33, 54–64], except the recent JLab data [65, 66], were used in the 2005 fit. As seen in Fig. 5, below 1 (GeV/c)² the data are inconsistently scattered even within individual data sets. The model tracks an average of the scattered data and fits the higher- Q^2 data well, dropping below the dipole values above $Q^2 = 4$ (GeV/c)². The newer data [66] are a little lower in the mid-range and this reinforces the tendency to go below the dipole fit.

Fig. 6 shows that G_E^n , just as G_E^p/G_D in Fig. 3 fits the data derived from polarization results of Fig. 4 very well. The values obtained from Rosenbluth separations [43, 54, 55,

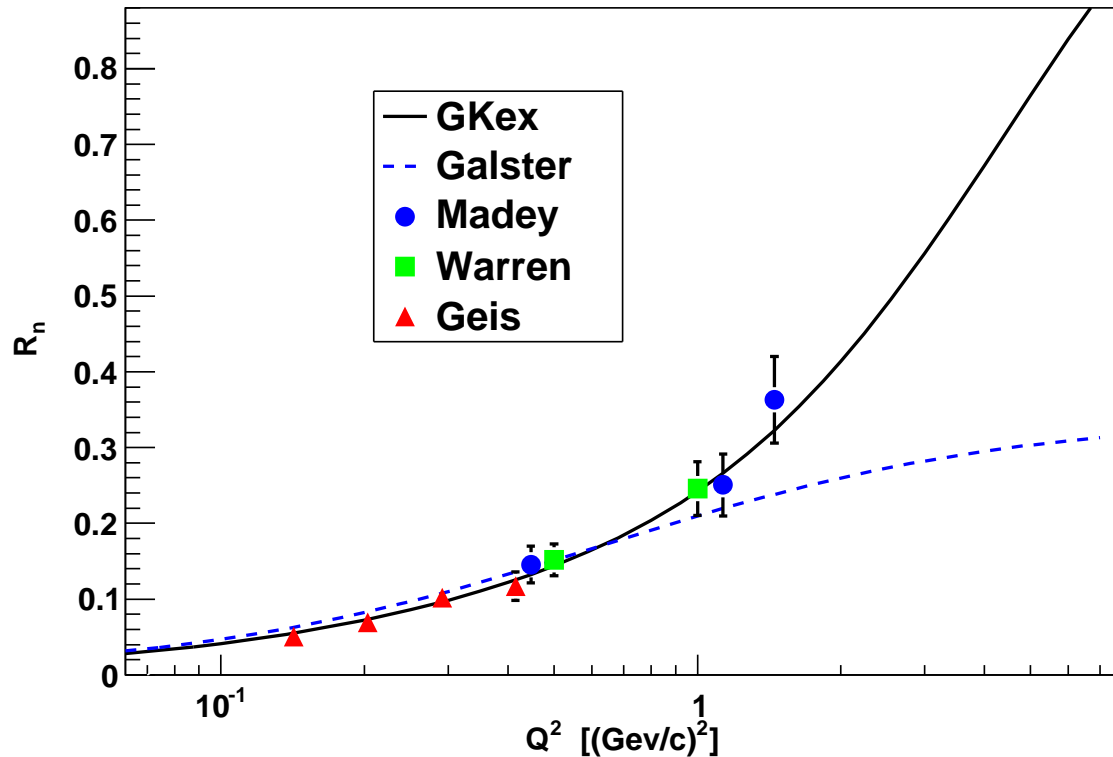


FIG. 4: Form factor ratio R_n with the GKex universal fit [23] and the Galster [24] parameterization with the fitted data (Madey [50] and Warren [51]; see the end of Sect: II) and recent results from BLAST (Geis [52]). In color online.

57, 67–75] would be much higher than those, but are not plotted because of their greater sensitivity to the two-photon corrections and the nuclear target model dependence.

Figures 1–6 show not only the data at low- Q^2 , the main focus of this study, but also over an expanded range to see the small structures in the data and models better. It is noteworthy that, while the parameters of this model were fitted using the whole momentum transfer region of the available data, the model reproduces the low momentum transfer BLAST data recently obtained (after the model fit) for Q^2 between 0.1 and 0.6 (GeV/c)² [38, 52]. These new data do not confirm possible “bump” structures near 0.2 (GeV/c)² suggested by earlier measurements and the invocation of a phenomenological pion cloud [76] is not required. In VMD-DR models, such as the ones discussed here, the pion cloud is represented by pion pairs and triplets largely clustered into vector mesons. This is consistent with the analysis of Hammer, Drechsel, Meissner [77] which shows that, after the imposition of unitarity, the

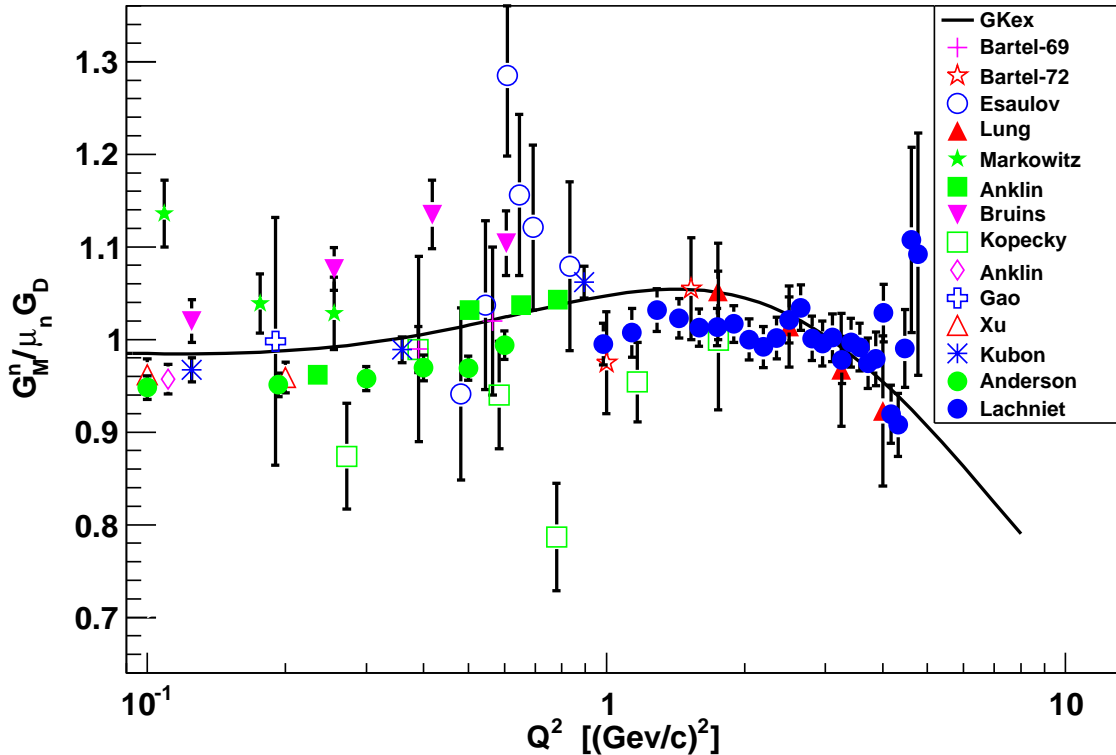


FIG. 5: The ratio $G_M^n/\mu_n G_D$ with the GKex universal fit [23] and the fitted data (Bartel-69 [54], Bartel-72 [55], Esaulov [56], Lung [57], Markowitz [58], Anklin [59], Bruins [60], Kopecky [33], Anklin [61], Gao [62], Xu [63], Kubon [64]; see the end of Sect: II) together with new results from JLab (Anderson [65] and Lachniet [66]). In color online.

addition of $\pi\pi$ continuum to that given by the ρ is insufficient to provide a substantial bump structure.

Finally, a few words are in order concerning the full GKex form factors and their pQCD terms. Because Λ_{QCD} is ≤ 200 MeV, it was initially expected that the asymptotic pQCD region would be approached at momentum transfers not much larger than 1 GeV/c [78, 79]. This may apply to inclusive reactions, but it was pointed out [80–82] that for exclusive processes the momentum transfer had to be shared among several exchanged gluons. It was then estimated that pQCD may not be approached for elastic form factors until the order of 1000 GeV/c. In fact for elastic proton-proton scattering the strong persistence of polarization effects [83] (which vanish in pQCD) at $T_{\text{lab}} = 28$ GeV involves much larger momentum transfers, up to 8 (GeV/c)².

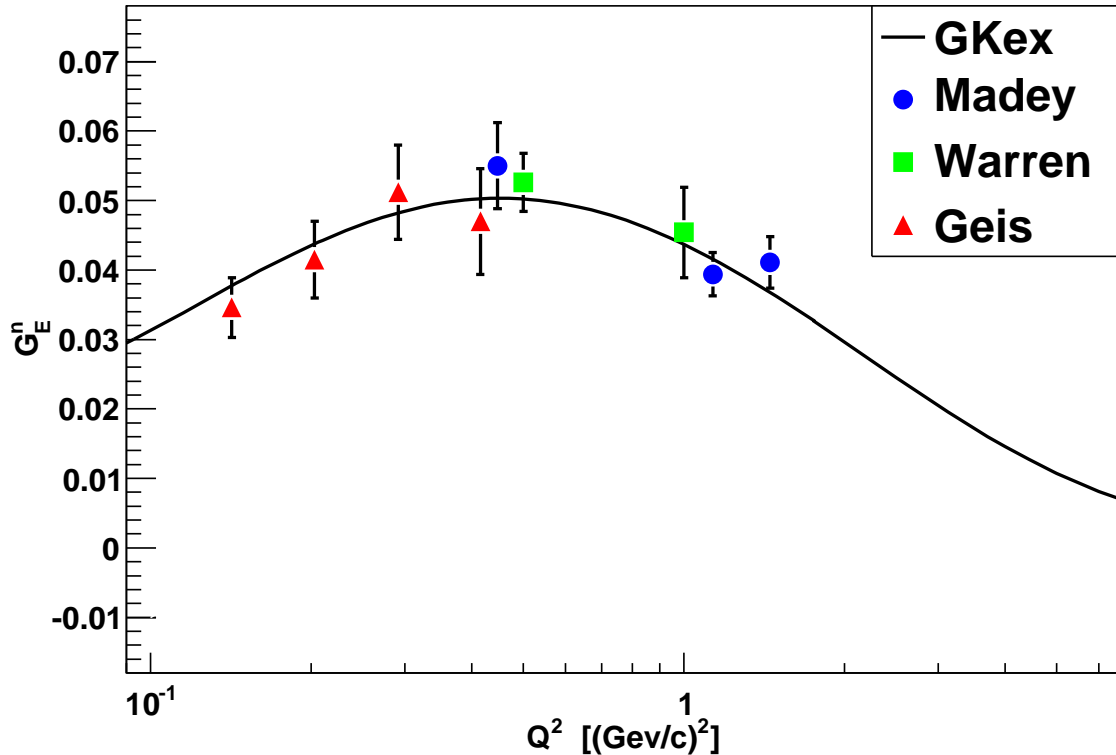


FIG. 6: G_E^n with the GKex universal fit [23]. The inconsistent G_E^n data from the unpolarized differential cross section fitted in [23] are not plotted here. The data points are translated from Fig. 4 through multiplication of R_n by G_M^n/μ_n . In color online.

For this model and its normalization of the pQCD limit, the magnetic form factors and pQCD are about 10% different at $Q^2 \sim 10$ (GeV/c) 2 . While R_p is within 10% of pQCD near 2 (GeV/c) 2 , R_n is only 80% of pQCD at 50 (GeV/c) 2 . Separating the isovector and isoscalar and the Dirac and Fermi terms gives a more specific indication of the slow approach to pQCD, as doing so minimizes accidental cancellations between terms. The isovector form factors $F_{1,2}^{(1)}$ are both relatively large. One finds that for $Q^2 < 5$ (GeV/c) 2 three of the four form factors are very different from the pQCD results alone — only $F_1^{(1)}$ is relatively similar to the pQCD contribution down to about 2 (GeV/c) 2 . As Q^2 increases beyond about 5 (GeV/c) 2 the pQCD contribution begins to saturate the total; specifically, at 10 (GeV/c) 2 the ratio of the pQCD contribution to the total is 96% for $F_1^{(1)}$ and 83% for $F_2^{(1)}$. The corresponding numbers at 20 (GeV/c) 2 are 98% and 88%, respectively. The isoscalar form factor $F_1^{(0)}$ is somewhat smaller than the isovector form factors and again shows saturation

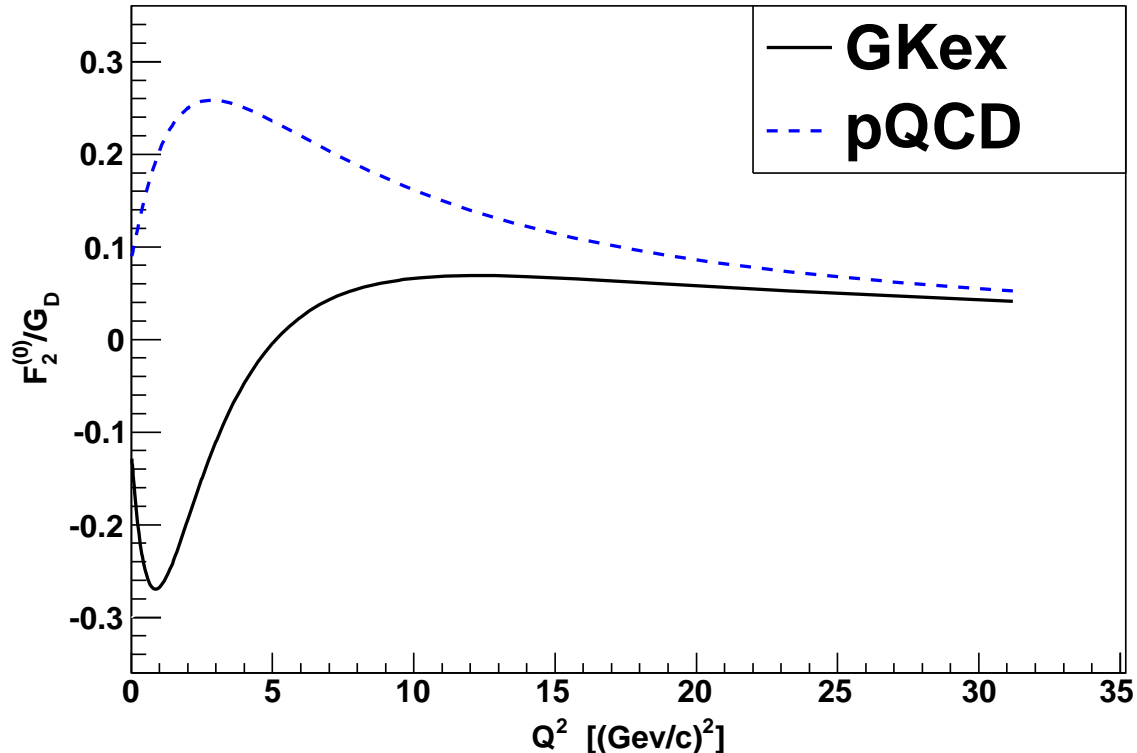


FIG. 7: The isoscalar Pauli form factor normalized to G_D with the GKex universal fit [23] (solid) and the pQCD term of that fit (dashed). In color online.

of the pQCD contribution with increasing Q^2 , although somewhat more slowly than for the isovector form factors. The ratio of the pQCD contribution to the total result for $F_1^{(0)}$ is 79% at 10 $(\text{GeV}/c)^2$ and 88% at 20 $(\text{GeV}/c)^2$. Finally, the isoscalar form factor $F_2^{(0)}$ is relatively small and slower to converge to the pQCD result (see Fig. 7). It should also be noted that the model curve for $F_2^{(0)}$ has a substantial dip near 1 $(\text{GeV}/c)^2$ which can be attributed to the opposite signs of the large ω and ω' magnetic contributions. In Sect. IV we show the individual contributions to the form factors, including those from the pQCD terms discussed here. The convergence is similar for the previous GKex model [21]. However, the pQCD normalization is expected to depend on possible major modifications of the model such as the addition of non-pQCD terms above the vector meson resonance region.

Finally, recently Belushkin, Hammer and Meissner [25] [BHM] have extended the Höhler-type model by considering the $K\bar{K}$ and 3π continua in addition to the 2π continuum, and conclude that the first two are adequately represented by including only simple poles and

adding a broad phenomenological contribution to each isovector form factor at higher masses. The asymptotic momentum transfer behavior is restricted by a super-convergent requirement in one fit, but by an explicit pQCD behavior in another version. As there are no hadronic form factors, the required asymptotic behavior is obtained by a restriction on the sum of all terms in the fit to the coupling strengths and masses. This results in requiring vector mesons with unobserved masses. The BHM-pQCD asymptotic behavior model requires fewer extra vector mesons than the BHM super-convergent (SC) model.

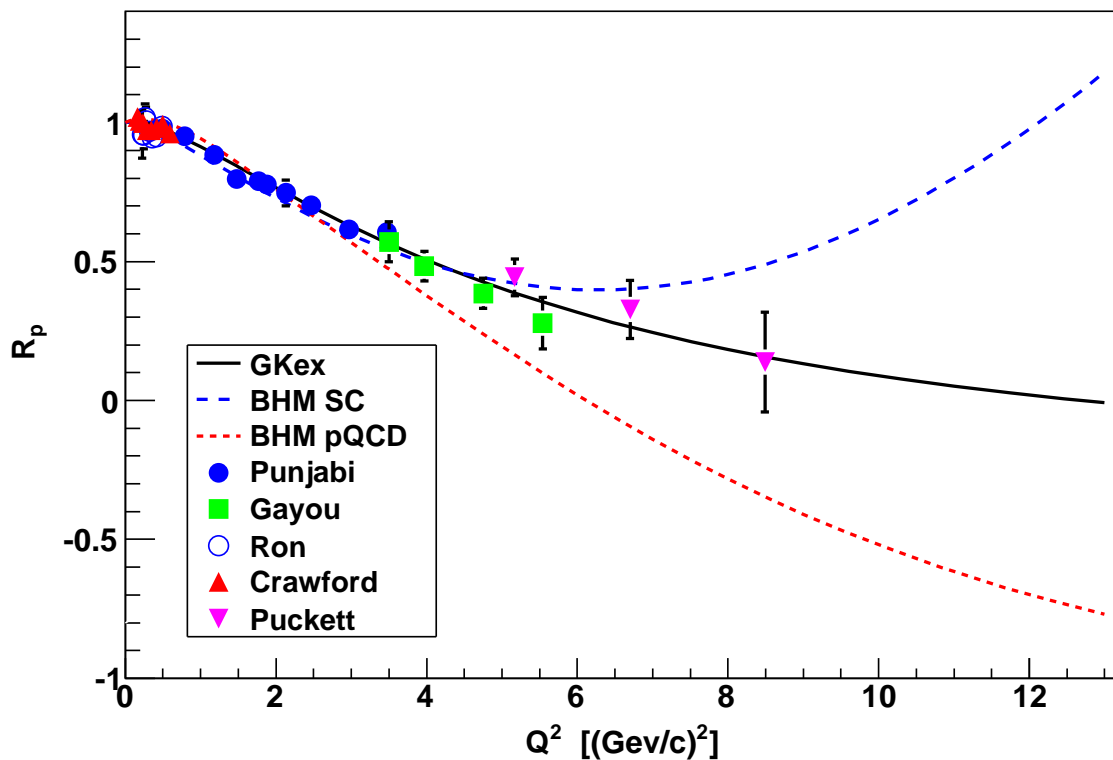


FIG. 8: R_p compared to the GKex [23] and BHM [25] super-convergent and asymptotically pQCD curves with the data as in Fig. 1. In color online.

Overall the GKex model agrees with the data better than do either the BHM-pQCD or BHM-SC models. Figure 8 illustrates the above remarks for R_p , where the GKex model follows the behavior of the data up to the highest available values of Q^2 , whereas in the high- Q^2 regime the other models differ substantially from the data.

Note that the BHM model is further constrained to fit time-like data. The previous version of the GKex model [21] was shown to provide a qualitative fit to the time-like data

by Tomasi-Gustafsson et al. [84] and a combined fit of the model to space- and time-like data is underway [85].

IV. INSIGHTS IN MOMENTUM SPACE WITHIN THE VMD + DR MODEL

In Figs. 9–12 the four types of form factors divided by the standard dipole form factor G_D are shown as functions of Q^2 over the range 0–2 (GeV/c)². Each is broken down into the individual contributions from the vector mesons and from the term that carries the asymptotic behavior, labelled pQCD. Several insights emerge from this GKex model representation. First, the ϕ and ρ' mesons do not play very important roles in this region of momentum transfer for any of the four types of form factors. Second, the ω' contribution is important for the electric form factors (Figs. 9–10), but less so for the magnetic form factors (Figs. 11–12). The ρ , ω and pQCD contributions are important in all cases. Note that for the electric form factors the ρ has a crossing at $Q^2 \sim 0.7$ (GeV/c)² which leads to interesting interplay with the other mesons, being constructive or destructive interferences depending on the region of momentum transfer of interest. The magnetic form factors in Figs. 11–12 yield a final result which is roughly dipole in shape over the region of momentum transfer shown in the figures (the results presented there are divided by the dipole form factor and so being dipole corresponds to having a flat curve). However, upon looking in more detail at the breakdown into the individual contributions, one sees that this arises essentially from the opposing behavior of the ρ and pQCD pieces. The ρ alone, for example, is more monopole in character, as discussed in Sect. II. The compensation is not complete, however, and the ω also plays a role in yielding the total. This leads to the total curves being flat at roughly the 5–8% level. In contrast, for G_E^p (Fig. 9) the ρ contribution wins and the net result falls faster than dipole, an explicit demonstration of what all VMD-type approaches have always predicted and now appears in the results obtained using polarization observables, as discussed above. Finally, for G_E^n shown in Fig. 10 the situation is even different: the ω and ω' compensate almost exactly to yield a dipole behavior, as they do for G_E^p , since these are isoscalar contributions and hence the same in the two cases; the pQCD contribution is flatter than in the other cases; and accordingly the ρ drives the rising behavior of G_E^n/G_D .

Finally, let us discuss the role of the ρ width. In Fig. 13 the ρ contributions are shown for G_E^p and G_M^p (for G_E^n and G_M^n the results are the same magnitude, but opposite signs,

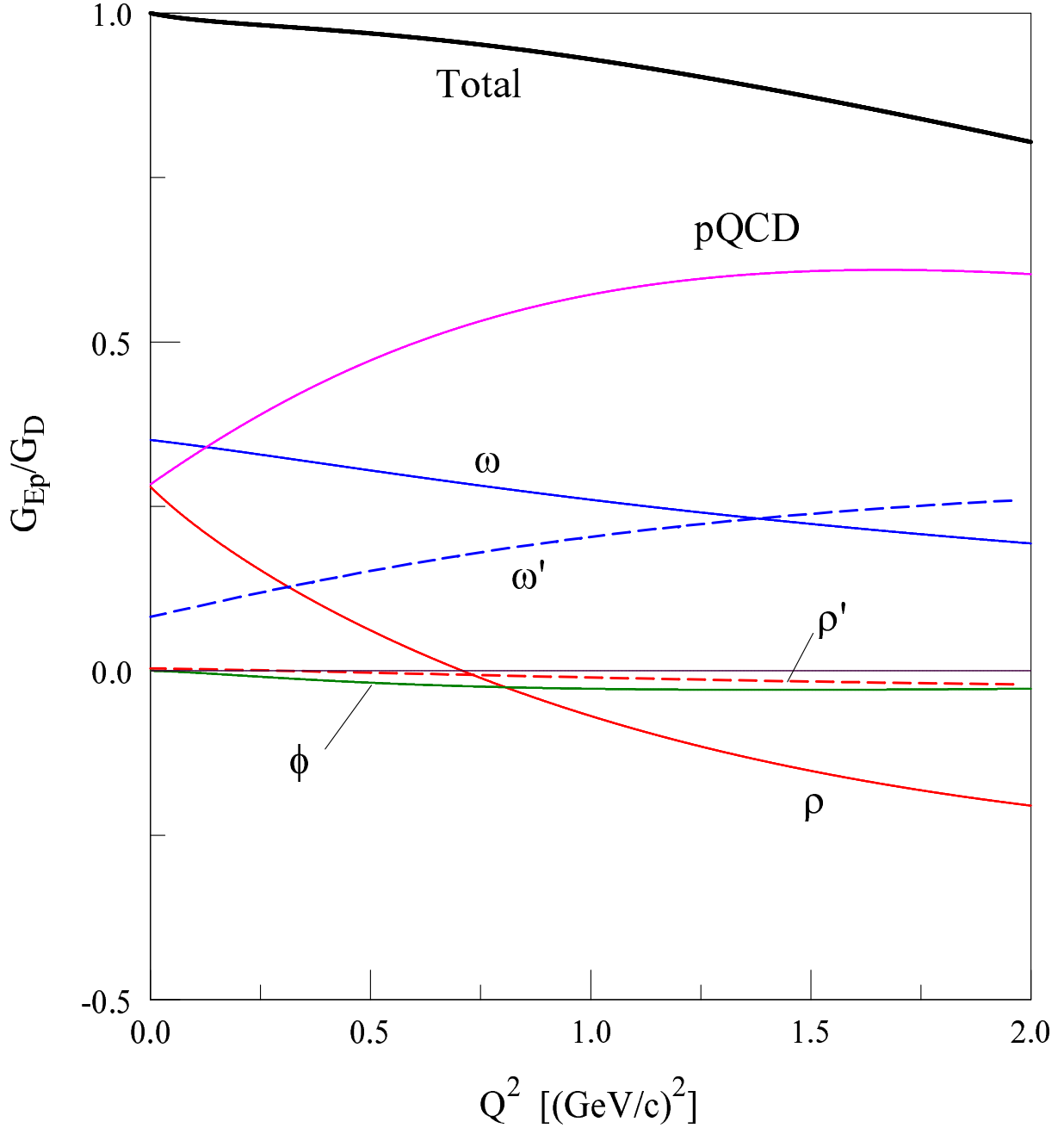


FIG. 9: G_E^p normalized to G_D showing the relative contributions of the various vector mesons from the GKex model together with the pQCD contribution. In color online.

since the ρ is isovector). The solid curves repeat the results shown in Figs. 9 and 11, while the dashed curves display what happens when the ρ width is set to zero and the mass is set to the physical mass of the ρ . In Sect. V A we return to see what consequences this has for the coordinate-space representations of the charge form factors.

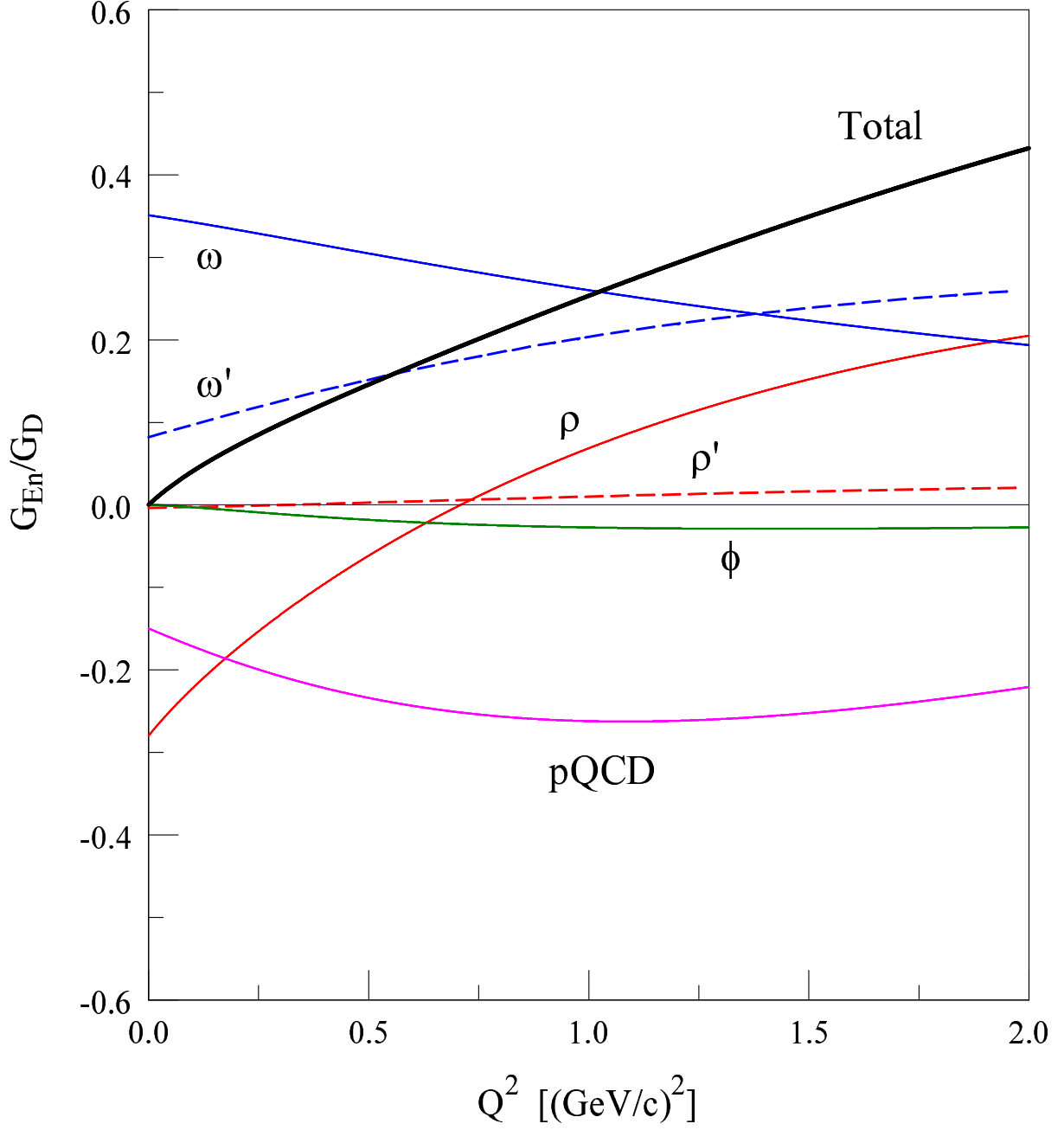


FIG. 10: G_E^m normalized to G_D showing the relative contributions of the various vector mesons from the GKex model together with the pQCD contribution. In color online.

V. REPRESENTATIONS IN COORDINATE SPACE

The discussion in this section is centered on transforming both what has been measured and the results from the GKex model for the electric form factors into coordinate space.

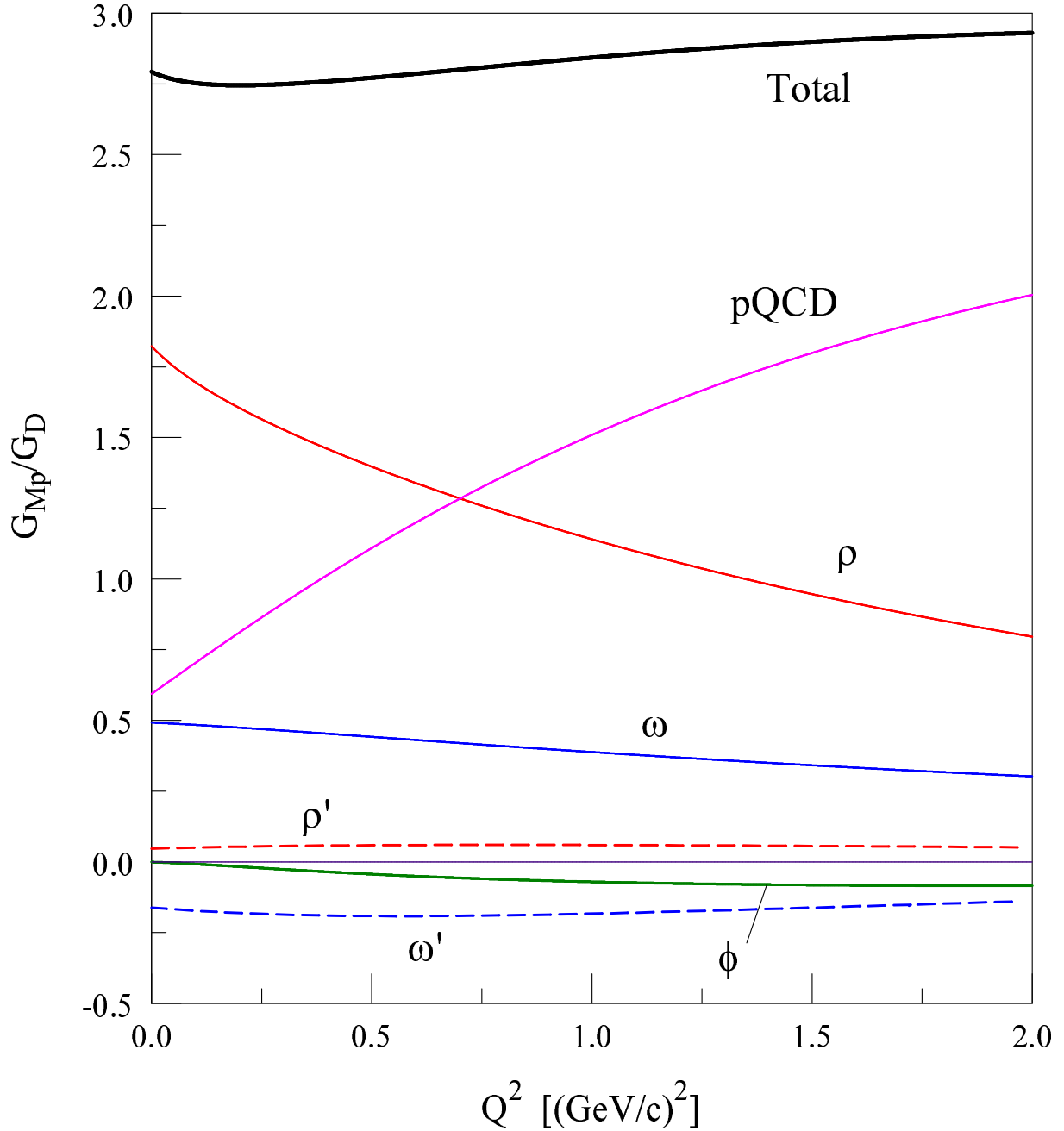


FIG. 11: G_M^p normalized to G_D showing the relative contributions of the various vector mesons from the GKex model together with the pQCD contribution. In color online.

Several motivations exist for doing this:

- We hope to obtain some insights into how charge is distributed in the nucleon;
- We are interested in how the various ingredients of the VMD+DR approach are man-

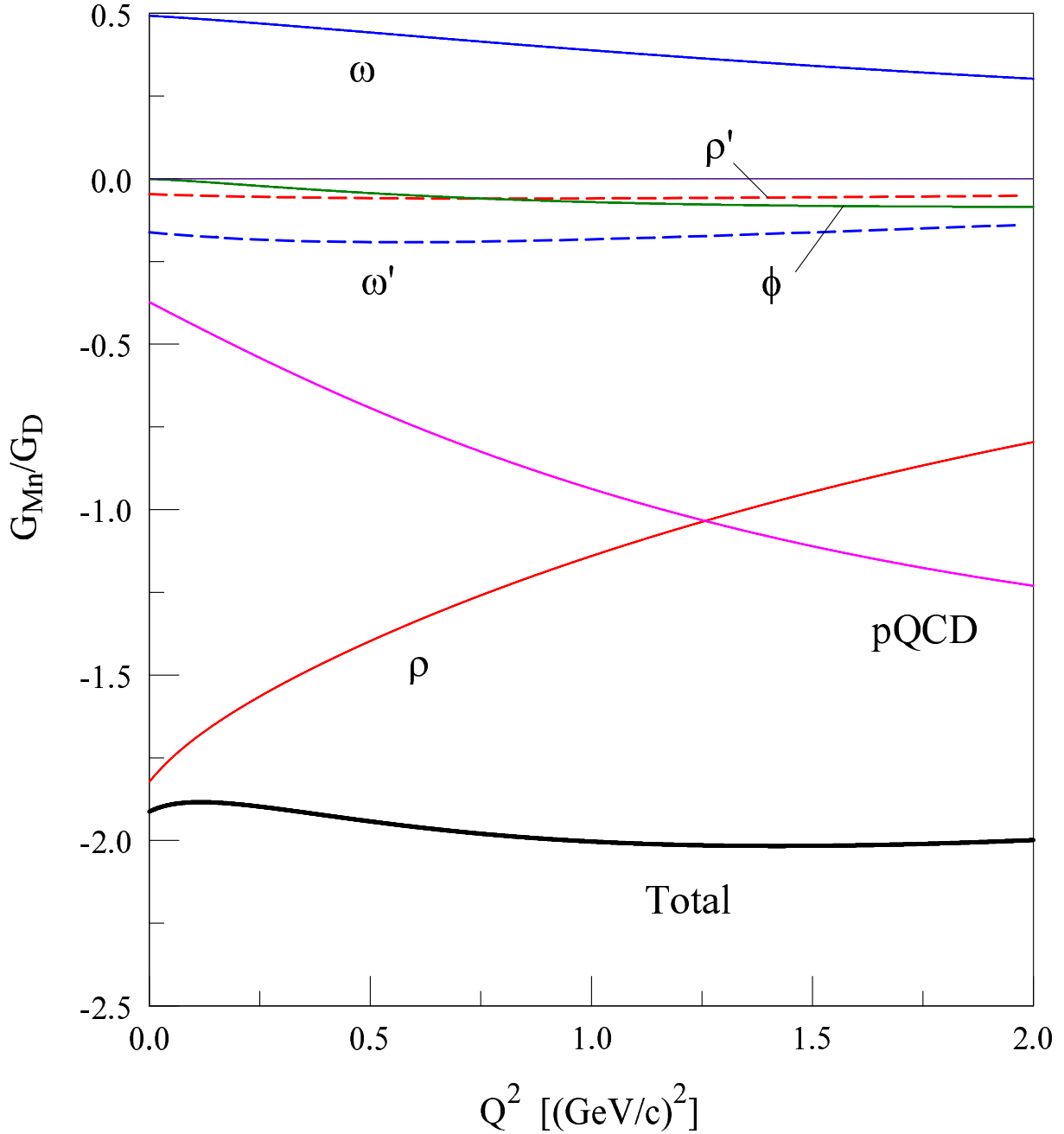


FIG. 12: G_M^n normalized to G_D showing the relative contributions of the various vector mesons from the GKex model together with the pQCD contribution. In color online.

ifested differently in coordinate space than they are in momentum space;

- In particular, we wish to explore the role played by the coupling to the continuum and thereby to gain some insights into, for instance, what roles pions play in determining the nucleon's form factors;

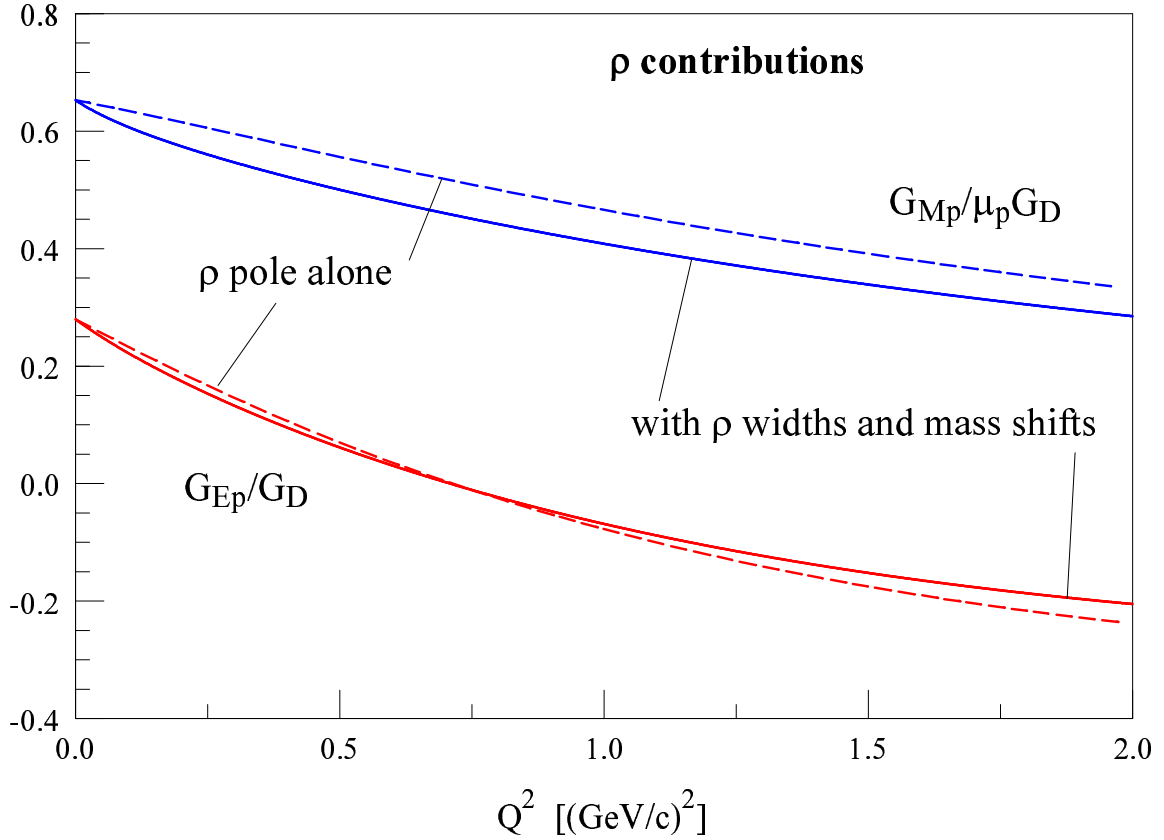


FIG. 13: G_E^p normalized to G_D and G_M^p normalized to $\mu_p G_D$ showing the ρ contributions from the GKex model with and without the widths and mass shifts. In color online.

- When characterizing the structure in coordinate space in terms of some set of basis functions the correlations which occur are different from those that enter when doing the characterization in momentum space and we hope to clarify this issue.

All of these are discussed in more detail below.

In context, note that a compromise is sometimes employed, that of Fourier transforming to coordinate space only with respect to the transverse directions (orthogonal to the boost), but leaving the third dimension in momentum space, thereby having a mixed representation [12]. While avoiding some of the inevitable problems discussed below, the nucleon's properties are harder to envision in this approach.

When choosing to represent the nucleon's properties one may choose any frame of reference, for instance, the initial-state rest frame, the final-state rest frame, choices in between

or frames boosted to the light-cone. Inevitably, however, the initial state, the final state or both states must be moving and therefore boosts are required when attempting to relate to properties in the nucleon rest frame. This makes the problem a relativistic one. Indeed, at high momentum transfers this makes the interpretation in terms of coordinate-space structure of the nucleon notoriously difficult, although at low enough momentum transfers it may be possible to make some connections between momentum and coordinate space. Problems occur in various guises, depending on the approach taken; for instance, rest frame models may be very difficult to boost and light-cone models can have troubles when boosting from the infinite momentum frame back to physical frames of reference.

Clearly it is important to choose the least relativistic frame of reference to optimize one's chances. This choice is the so-called Breit frame, as may be seen simply by minimizing the product of the boost factors

$$\begin{aligned}\gamma_i &= E_i/m_N \\ \gamma_f &= E_f/m_N\end{aligned}\tag{31}$$

for the boosts involved in relating the moving initial and final nucleon states to their rest frames. One has

$$p_f = -p_i = q/2\tag{32}$$

$$\omega = 0 \leftrightarrow \sqrt{|Q^2|} = |\mathbf{q}|\tag{33}$$

$$\gamma_f = \gamma_i \equiv \gamma_{Breit} = \sqrt{1 + \tau},\tag{34}$$

that is, the resulting Breit frame has the initial- and final-state nucleons moving with $\mp\mathbf{q}/2$, where \mathbf{q} is the 3-momentum of the virtual photon involved in the electron scattering process. The energy transfer that results is zero and hence $Q^2 = |\mathbf{q}|^2 = q^2$. One may then define the Breit-frame electric distributions as the Fourier transforms

$$4\pi r^2 \rho_{Breit}^{p,n}(r) \equiv \frac{2}{\pi} \int_0^\infty dq \, qr \sin qr \, G_E^{p,n}(Q^2)|_{Breit}.\tag{35}$$

Note that this is only a definition. For the reasons mentioned above, the resulting functions are not generally to be interpreted as the proton and neutron charge distributions, although they are perfectly well-defined quantities.

To obtain some feeling for where the interpretations as charge distributions clearly should be invalid (and therefore for where they may be reasonable) it helps to compare the Compton

wavelength $\lambda_C = \hbar c/Mc^2 \cong 0.21$ fm, where M is the mass of the nucleon, with the characteristic scale probed at a given momentum transfer $\lambda(q) \sim \hbar c/q$. These become equal when $q \sim 1$ GeV/c, and thus one must expect functional dependence at even higher momentum transfers or, corresponding, smaller distance scales to lie beyond simplistic non-relativistic intuition. At lower momentum transfers — corresponding to distance scales significantly larger than the nucleon’s Compton wavelength — there may be some validity to the interpretation of the coordinate-space distributions as charge or spin distributions. An insightful discussion of what toy models have to offer in this long-wavelength regime is contained in [86].

A. Insights obtained using the Breit-Frame Fourier Transform of the GKex Model

In Figs. 14–15 we show the Breit-frame Fourier transforms of the charge (electric) form factors of the proton and neutron, respectively, together with the individual contributions from the vector mesons and the asymptotic (pQCD). That is, the figures show the Fourier transform of the GKex model results discussed in Sect. IV. For the totals (the entire GKex model form factors) one has results which integrate to 1 (0) for the proton (neutron), since what is plotted is $4\pi r^2$ times the Breit-frame Fourier transforms. For the neutron one sees a positive contribution at small distances and a negative one at large distances, which is consistent with the fact that the mean-square radius for the neutron is $\langle r^2 \rangle_{En} = -0.115 \pm 0.0035$ fm² [33]. This is also consistent with a simple picture where isovector mesons such as the π and ρ extend to large distances and form the “meson cloud”. For example, although unrealistically simple, a model where a neutron spends part of its time as a “proton + negative pion” would yield just such a charge polarization, and not the reverse with a negative “core” and a positive “cloud”. Again, one is cautioned not to interpret these distributions as charge or spin distributions, except perhaps for their large-distance behavior. The issue of interpreting the rms charge radius of the neutron is discussed in [86].

Let us now discuss the individual contributions in somewhat more detail. As before the ρ' and ϕ contributions are seen to be very small, while the rest of the contributions play important roles. For the Breit-frame Fourier transform of G_E^p (Fig. 14) these mostly add together to form the total, whereas for the Breit-frame Fourier transform of G_E^n (Fig. 15) the isoscalar mesons “fight” against the isovector mesons and the pQCD term to yield a

relatively small net result. In both cases the longest-range effects arise from the ρ and next from the ω , while the ω' and pQCD contributions lie at small distances. Indeed, beyond about 0.7 fm most of the Breit-frame Fourier transform of G_E^p is contained in the ρ and ω alone (the neutron case is more complicated, due to the delicate cancellations seen in the figure).

The effect of “turning off” the ρ width was discussed in Sect. IV for the momentum-space GKex model results. Here we consider the Breit-frame Fourier transform as well. In Fig. 16 curves are shown for the ρ contributions in the proton both with the width included (solid curve, as in Fig. 14) and with it set to zero and the mass of the ρ set to its physical value (dashed curve). The latter is seen to have a bit more strength at smaller distances, although the effect is not pronounced. In the GKex representation of the form factors the only place that contributions from pions appear explicitly is via the width the ρ takes on, *i.e.* through connections to the $\pi\pi$ -continuum. Otherwise only vector mesons and the asymptotic form occur in the model. Thus, turning off these ρ -width contributions effectively eliminates explicit pions from the problem, and one must conclude that the latter are relatively unimportant.

B. Results in Coordinate Space

Again, given the caveats discussed in the introduction to this section, the world data for $G_E^{p,n}$ may be Fourier-transformed using Eq. (35). In order to obtain Fourier transforms of the experimental data, the world data of G_E^p and G_E^n were fit to various parameterizations which were then transformed numerically. Earlier work presented in the DOE/NSF NSAC Long Range Plan [87] was based on the data and parameterization used in [38, 52]. For the proton, this was the 6-parameter phenomenological fit function of [76] fit to the data from [35, 37, 38, 42, 43, 88–93]. For the polarized data, G_E^p was obtained by combining the form factor ratio with the Kelly [94] fit of G_M^p . For the neutron the fit function was reduced to the sum of two dipoles, fit to the data of [51, 52, 68, 69, 71–73, 75, 95–98]. The charge of the neutron was constrained to zero, leaving three free parameters. The RMS charge radius squared of [33] was included in the fit as an extra datum, not as a constraint. Figs. 17 and 18 show the Fourier transforms of these fits.

The error bands in Figs. 17 and 18 were obtained by combining the variation from each fit

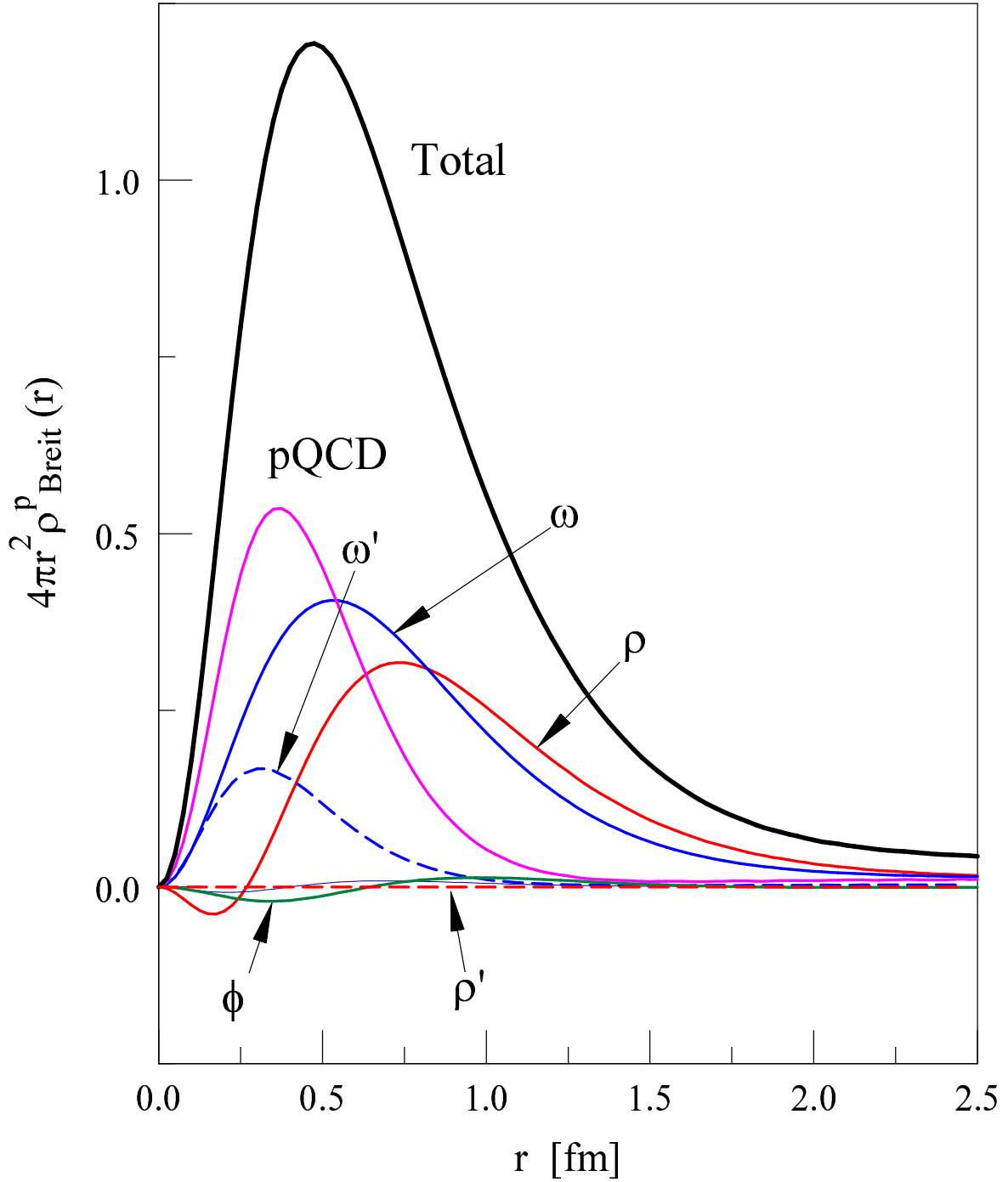


FIG. 14: $4\pi r^2 \rho_{Breit}^p(r)$ showing the relative contributions of the various vector mesons from the GKex model together with the pQCD contribution. In color online.

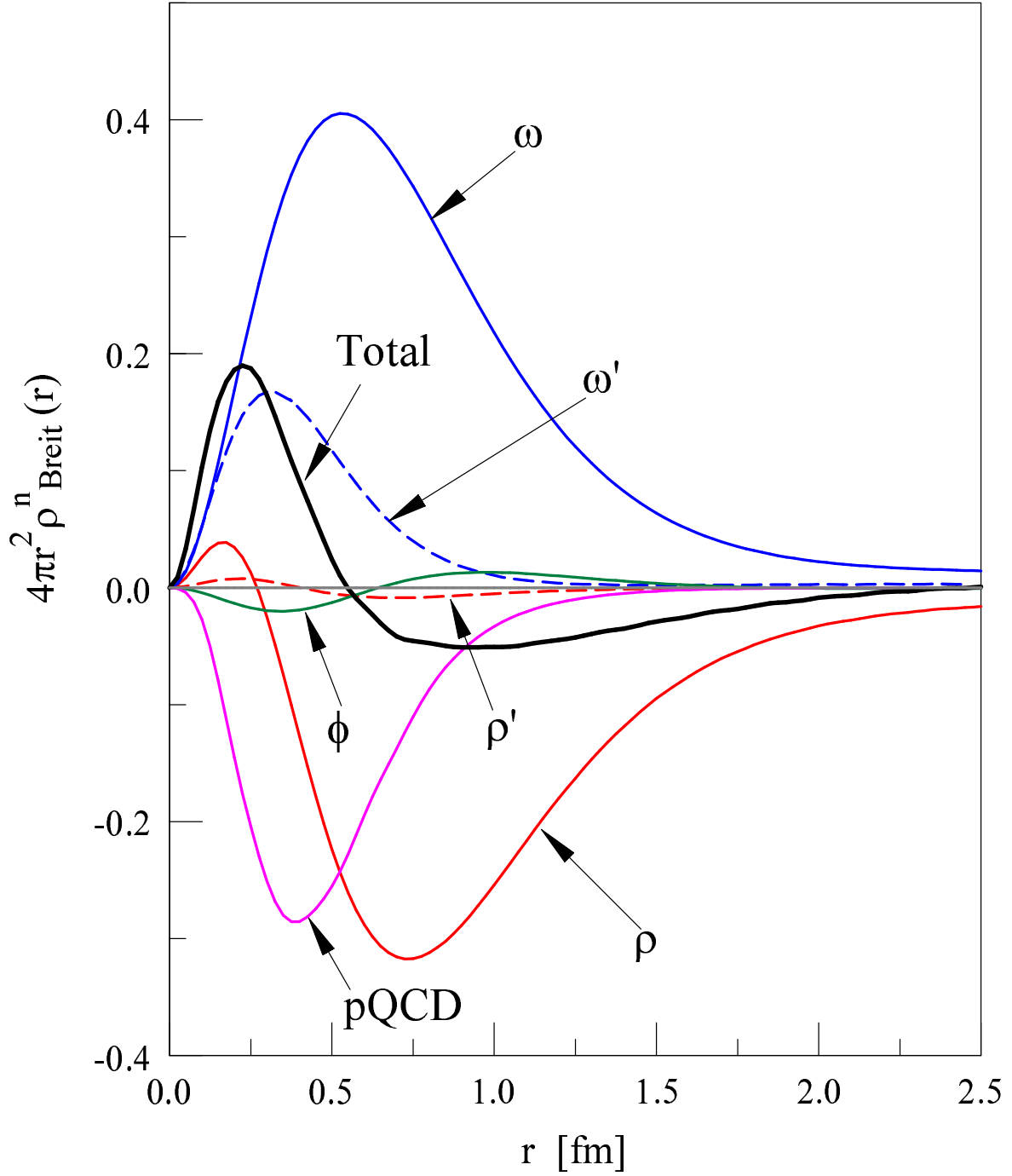


FIG. 15: $4\pi r^2 \rho_{Breit}^n(r)$ showing the relative contributions of the various vector mesons from the GKex model together with the pQCD contribution. In color online.

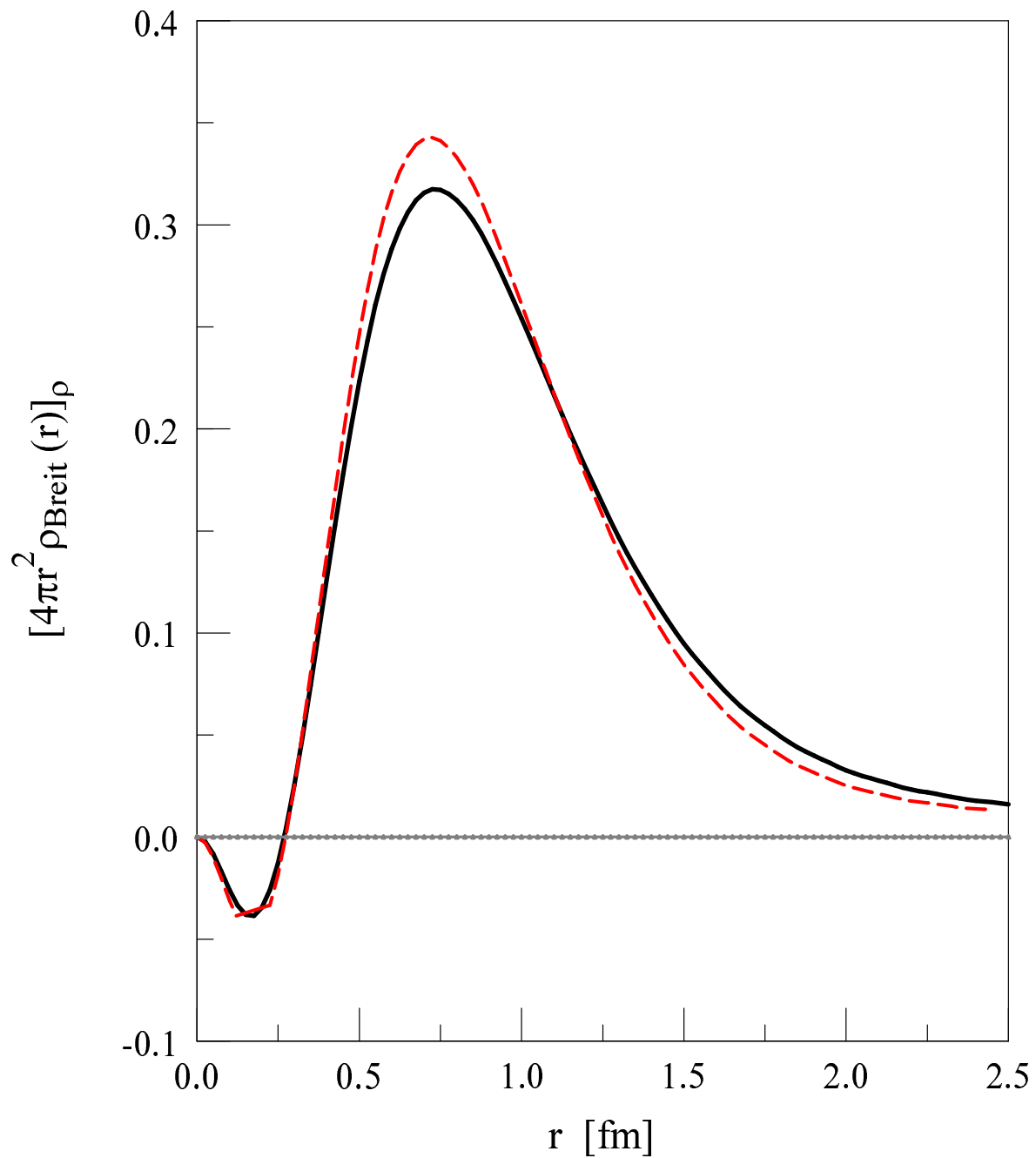


FIG. 16: $4\pi r^2 \rho_{Breit}^p(r)$ showing the ρ -meson contribution from the GKex model with the width included (solid curve), and with the width turned off and the mass set to the physical ρ mass (dashed curve). In color online.

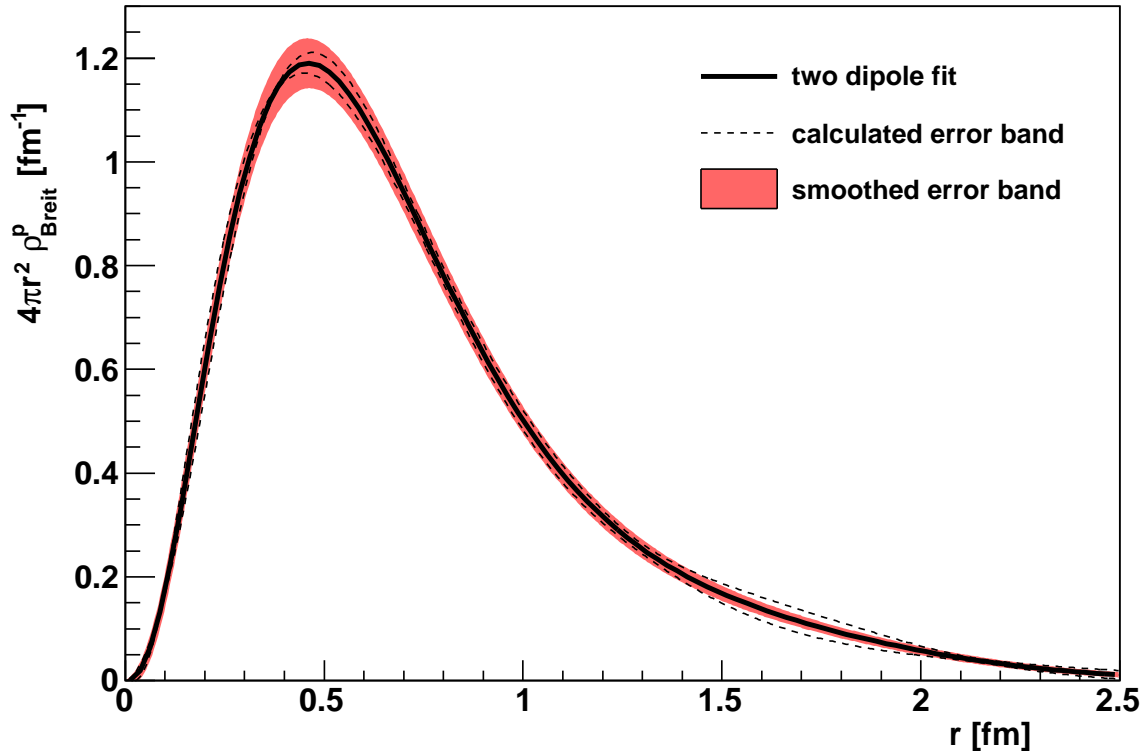


FIG. 17: Breit frame Fourier transform of G_E^p , as appeared in the long range plan [87], with both the calculated and smoothed error bands. In color online.

parameter with the full covariance matrix. The calculated error bands, shown with dotted lines, have large oscillations in width, even dropping to $\delta\rho_{Breit} \sim 0$ around $r=0.37$ fm for the proton and $r=0.75$ fm for the neutron. The calculated uncertainty for the proton also gets significantly smaller around $r=0.75$ fm. This is clearly model dependence: the Fourier transform of this particular model has no flexibility at that point to respond to variations in the data. The shaded error bands in Figs. 17 and 18, were smoothed out to account for the model dependence, producing the error bands, which appeared in [87].

This surprising behavior illustrates an interesting point, that a family of curves which fit the data well in momentum space may contain very little information or coverage of coordinate space. In choosing an appropriate model, one typically searches for the smoothest family of curves that fit the data with a reasonable χ^2 . In contrast, the Fourier transform inherently includes information on all frequencies, not just smooth low frequencies. For example, the fit to a constant function $f(k) = a$ only determines a single point at the

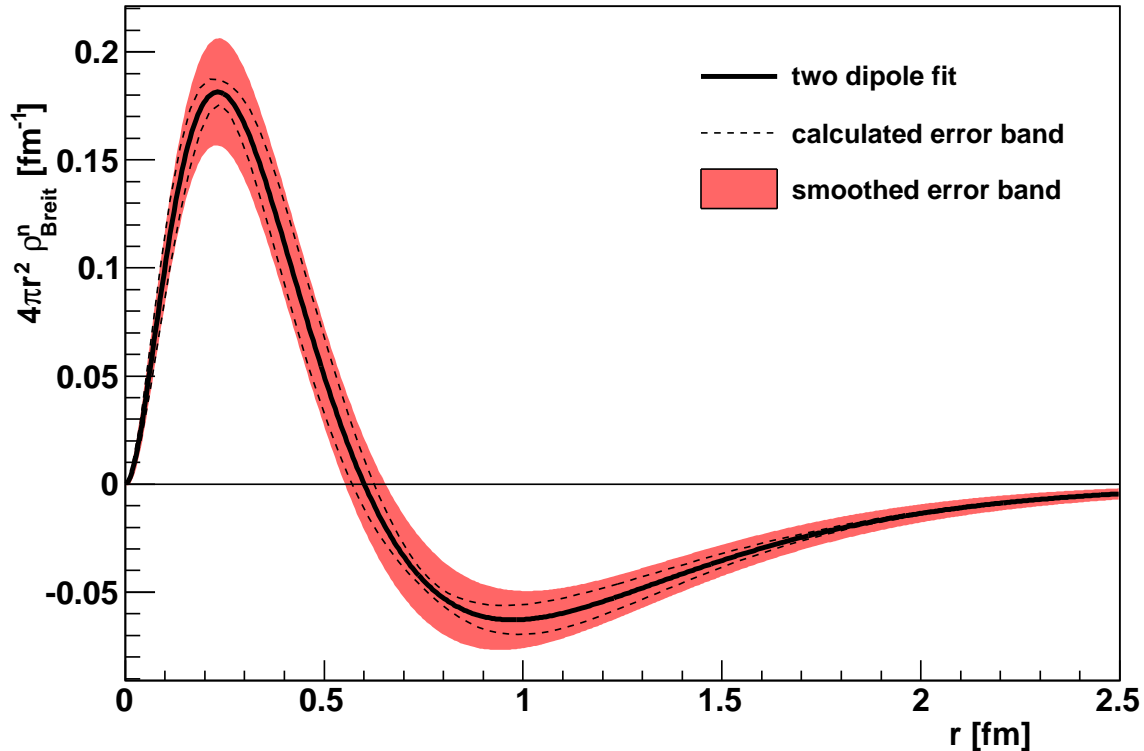


FIG. 18: Breit frame Fourier transforms of G_E^n , as appeared in the long range plan [87], with both the calculated and smoothed error bands. In color online.

origin of the Fourier transform $\tilde{f}(x) = a\delta(x)$. Even arbitrary fit functions in one parameter can often be approximated by $f(k) = g(k) + a$ for a fixed function $g(k)$. In momentum space, that function will have a uniform error-band over the entire domain, but that error is completely correlated along the entire function. The Fourier transform has non-zero error bars only at the origin in position space.

To obtain a reasonable Fourier transform with meaningful error bands, it is necessary to fit a function which spans both position and momentum space. This can be done by expanding the form factors in an orthogonal set of basis functions $\sum_{n=0}^N \tilde{f}_n(k)$, using the simple prescription $Q^2 = \hbar^2 k^2$. The kernel of the Fourier transform is unitary, ensuring an expansion $\sum_{n=0}^N f_n(r)$ in orthogonal basis functions in position space also. Following Kelly [99, Eqs. (28, 29)], we fit the data to two orthogonal basis functions. The first is the Fourier-Bessel Expansion (FBE), the wave functions of an infinite spherical well of radius

R_{max} in position space,

$$f_n(r) = j_0(k_n r) \Theta(R_{max} - r), \quad (36)$$

$$\tilde{f}_n(k) = \frac{(-1)^n R_{max}}{k^2 - k_n^2} j_0(k R_{max}). \quad (37)$$

$$(38)$$

These functions are localized in frequency, peaking at $k_n = n\pi/R_{max}$, with a hard cutoff at the n -th zero of the $l = 0$ spherical Bessel function $j_0(x)$ at R_{max} . The second is the Laguerre-Gaussian expansion (LGE), the wave functions of a spherical harmonic oscillator of frequency $\omega = 2\hbar/mb^2$ for fixed parameter b ,

$$f_n(r) = e^{-x^2} L_n^{1/2}(2x^2), \quad (39)$$

$$\tilde{f}_n(k) = \frac{\sqrt{\pi}}{4} b^3 (-1)^n e^{-y^2} L_n^{1/2}(2y^2), \quad (40)$$

$$(41)$$

where $x = r/b$, $y = kb/2$, and $L_n^{1/2}$ is a generalized Laguerre function. These functions are localized in neither position nor momentum. The width of the basis functions is not fixed in coordinate space, but increases with n as $b\sqrt{n}$. Higher-order functions emphasize larger values of both r and k . These two basis sets have quite complementary features; so it should be clear by comparing results from the two expansions which parts depend on the particular basis set used and which are model-independent. In this paper, relativistic corrections to the form factors or to $Q^2 = \hbar^2 k^2$ are not considered as they were in [99].

There are a number of sources of uncertainty in the fits, which are interrelated. The maximum value of Q^2 of the data limits the maximum number, N , of basis functions which can be fit for fixed R_{max} or b . The Q^2 range of each basis function depends on R or b so a larger number of basis functions can be used by increasing the size of the box. However the box size is limited by the Q^2 gaps in the G_E^p and G_E^n database. With the appropriate box size, N is ultimately limited by the finite number of form factor measurements at independent values of Q^2 . If one tries to use more basis functions, the fit parameters will become highly correlated, manifest by a large error band. Even below this limit, as N increases there are fewer data per fit parameter, and so the error should grow as \sqrt{N} . This increase in error is offset by the extra information obtained in higher spatial frequencies. The truncation error from omitting higher frequencies is represented below with a horizontal error bar of width

$\delta r = h/4\sqrt{Q^2}$, a quarter wavelength of the highest frequency basis function. This is an overestimate, since the form factors fall off rapidly with Q^2 .

With the small number of basis functions ($N=7-8$) afforded by the data, it is difficult to obtain convergence to $G_E^{p,n}(Q^2)$. Better convergence can be obtained while retaining the model independence by fitting only the residual form factors after subtracting an arbitrary base function which reproduces the general features of the data. We used the GKex model as the base function. The FBE or LGE expansion is used to fit the small correction to GKex from the data, and mainly to calculate the model-independent error band of the Fourier transform. The quality of the base function can be assessed by comparing the residual fit with the size of the error band. The model independence can be shown by comparing the FBE and LGE expansions, and by using different base functions.

In general, the widths of the error bands of the fits to $4\pi r^2 \rho^{Breit}(r)$ were linear in r , superimposed with an oscillation due to truncation after a finite number of the basis functions. The oscillations were approximately the frequency of the highest basis function. The linear part was consistent between the FBE and LGE residual fits, but not the oscillations. The oscillations were small for reasonable values of N , but started to dominate as too many basis functions were used. Only the linear part of the error bands were used in the final plots.

The complete procedure used to determine the optimal values of the non-fit parameters (Q_{max}^2, N, R_{max}) or (Q_{max}^2, N, b) in the Fourier transform of the data is as follows. The residual $G_E^{p,n}(Q^2)$ data after subtracting the GKex model were fit to a series of N basis functions, either FBE or LGE. The width of the error band was fit to the linear function $\delta\rho(r) = \rho_1 \cdot r / 1 \text{ fm}$, and then $\rho_1(N)$ was plotted as a function of the number of basis functions used each fit. A series of such plots $\rho_1(N; Q_{max}^2)$ was generated for data subsets with different cuts of the form $0 < Q^2 < Q_{max}^2$. The values $Q_{max}^2 = 0.1, 0.4, 0.7, 1.0, 1.5, 2.0, 3.0,$ and 6.0 (GeV/c)^2 for the proton and $Q_{max}^2 = 0.2, 0.3, 0.5, 1.0,$ and 1.5 (GeV/c)^2 for the neutron were used to generate the series of plots. At small N , $\delta\rho(N)$ was the same for each value of Q_{max}^2 . As N increased, $\delta\rho(N)$ began to diverge for data sets with lower values of Q_{max}^2 . The threshold of N where the fits began to diverge indicated the maximum number of basis functions feasible for each Q^2 range, $N(Q_{max}^2)$. The Q^2 range was fixed at $Q_{max} = 1.5 \text{ (GeV/c)}^2$ for comparison of $\rho_{Breit}^p(r)$ and $\rho_{Breit}^n(r)$ and to avoid issues of two photon contributions. The entire procedure was repeated with different box sizes R_{max} (FBE) or b (LGE). The values R_{max} and b were chosen to minimize $\delta\rho_1(N, Q_{max}^2)$. As one would

expect, the optimal box size was the same for the proton and neutron. The best value of R_{max} was the same as in Kelly [99]; however, the best value for b was about twice as large. The parameters obtained using this procedure are listed in Table I.

FF	Q_{max}^2	N	R_{max}	b
G_E^p	1.5 (GeV/c) ²	8	4 fm	1.05 fm
G_E^n	1.5 (GeV/c) ²	7	4 fm	1.11 fm

TABLE I: Fixed parameters used in the fits of FBE and LGE basis function to the residual $G_E^{p,n}(Q^2)$ after subtracting the GKex model.

In Figs. 19 and 20, $\rho_{Breit}(r)$ for the GKex model is compared with fits to the world data with smoothed error bars obtained through the above procedure. The differences between the solid curve and the two other curves are the LGE and FBE residuals fitted to the data. The residuals are small, but statistically significant. Although they deviate from the GKex model, the FBE and LGE residuals are consistent with each other within error. This is an important confirmation of the model-independence of the residual fit, since the two basis functions are very different, as described above. To check for coverage of the basis functions, fits to the residuals of different parameterizations such as the F-W or two dipole forms from above were compared with GKex+FBE and GKex+LGE and found to be consistent within error. We conclude that the Fourier transforms of G_E^p and G_E^n world data are robust with realistic error bands. To place these Breit-frame distributions in context with other work, note that when representing results in the light-cone frame, for instance, that different (but not incompatible) behaviors may emerge, showing that one's perceptions must be keyed to what frame of reference is chosen. Examples of this type may be found in the work of [13, 22, 100] where the light-cone-frame neutron distribution may even be negative at the origin.

The Breit coordinate-space electric distributions discussed above may be combined to yield two different quantities. First, by taking sums and differences the isoscalar and isovector Breit-frame electric distributions shown in Fig. 21 may be constructed:

$$\rho_{Breit}^s(r) \equiv \rho_{Breit}^p(r) + \rho_{Breit}^n(r) \quad (42)$$

$$\rho_{Breit}^v(r) \equiv \rho_{Breit}^p(r) - \rho_{Breit}^n(r). \quad (43)$$

Since the neutron electric distribution shown in Fig. 20 is positive at small distances and

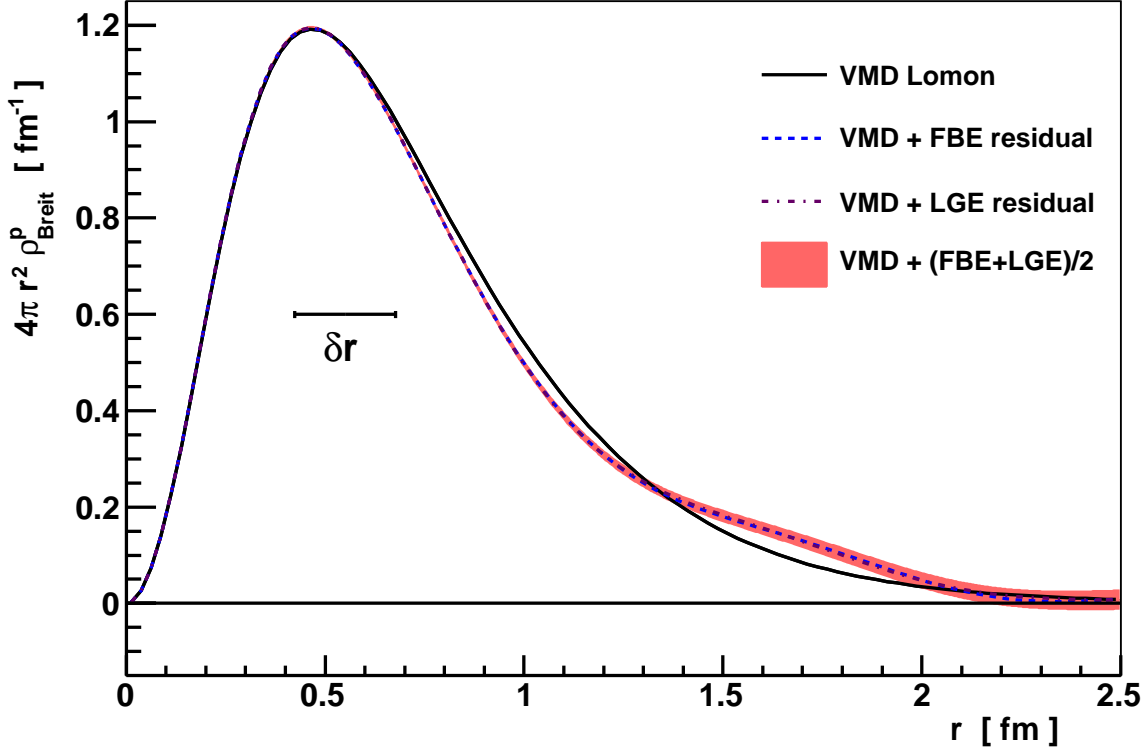


FIG. 19: Coordinate-space representation $4\pi r^2 \rho_{\text{Breit}}^p(r)$ obtained using Eq. (35) with $G_E^p(Q^2)$ together with the GKex VMD model of Lomon [23]. In color online.

negative at large distances one sees that the isovector distribution lies outside the isoscalar one, apparently consistent with isovector mesons playing an important role in determining the large-distance behavior (compare Fig. 21 with Figs. 14 and 15 where one sees the ρ contribution extending beyond the ω contribution).

Secondly, note that the proton and neutron Breit-frame electric distributions may be written in terms of Breit-frame electric up and down quark distributions (neglecting strange quark contributions), involving the appropriate numbers of quarks (1 or 2) and quark charges ($-1/3$ and $2/3$), both for the proton and for the neutron:

$$\rho_{\text{Breit}}^p(r) \equiv 2\left[\frac{2}{3}\rho_{\text{Breit}}^u(r)\right] + \left[-\frac{1}{3}\rho_{\text{Breit}}^d(r)\right] \quad (44)$$

$$\rho_{\text{Breit}}^n(r) \equiv 2\left[-\frac{1}{3}\rho_{\text{Breit}}^u(r)\right] + \left[\frac{2}{3}\rho_{\text{Breit}}^d(r)\right]. \quad (45)$$

Here ρ^u (ρ^d) denote up (down) quark distributions in the proton; by charge symmetry these are assumed to be the same as the down (up) quark distributions in the neutron to obtain

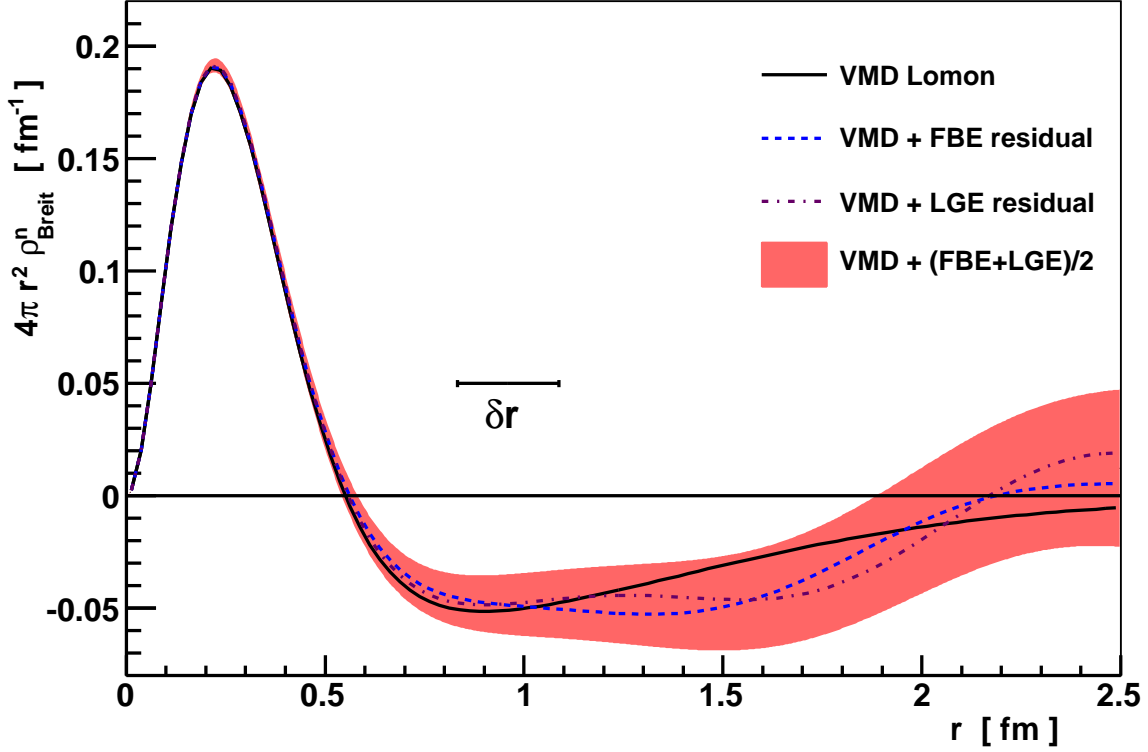


FIG. 20: Coordinate-space representation $4\pi r^2 \rho_{\text{Breit}}^n(r)$ obtained using Eq. (35) with $G_E^n(Q^2)$. In color online.

Eq. (45), *i.e.* we have assumed that

$$\rho^u \equiv \rho^{u(p)} = \rho^{d(n)} \quad (46)$$

$$\rho^d \equiv \rho^{d(p)} = \rho^{u(n)}. \quad (47)$$

Inverting, one may construct the corresponding up and down quark distributions in terms of the proton and neutron distributions

$$\rho_{\text{Breit}}^u(r) \equiv \rho_{\text{Breit}}^p(r) + \frac{1}{2}\rho_{\text{Breit}}^n(r) \quad (48)$$

$$\rho_{\text{Breit}}^d(r) \equiv \rho_{\text{Breit}}^p(r) + 2\rho_{\text{Breit}}^n(r), \quad (49)$$

shown in Fig. 22.

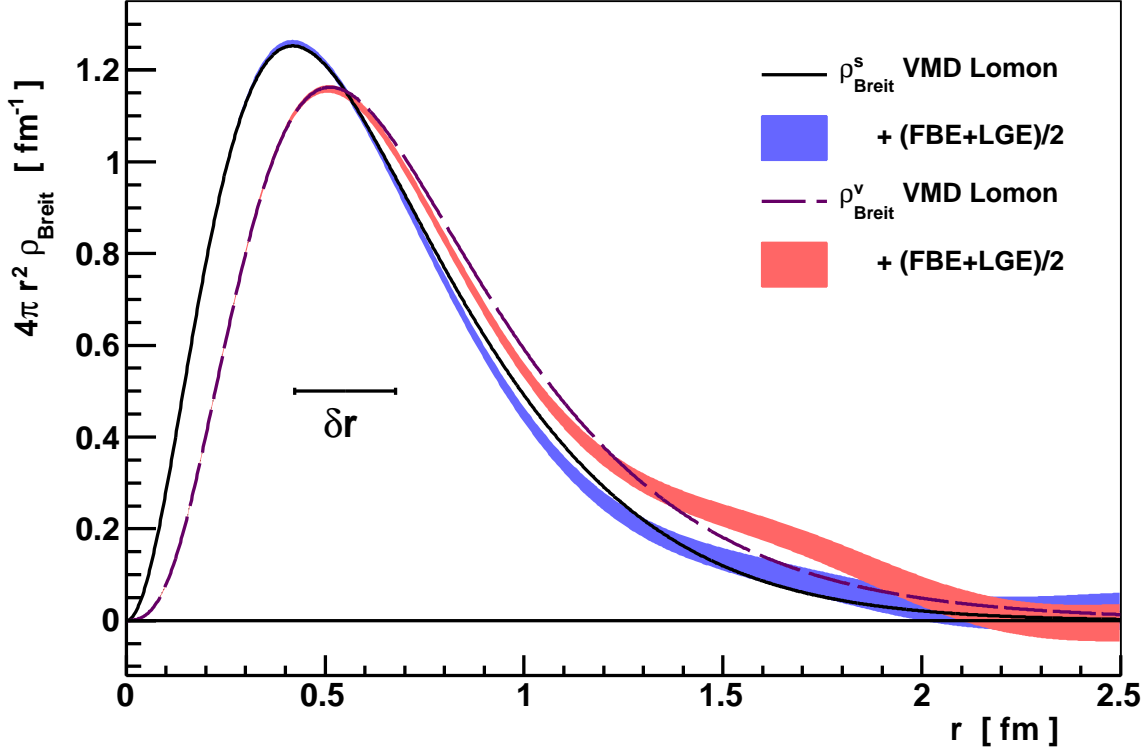


FIG. 21: Isoscalar and isovector coordinate-space electric Breit-frame distributions obtained using Eqs. (42) and (43). In color online.

VI. CONCLUSIONS

The goal of the present study has been to gain insight into the roles played by mesons in the electromagnetic form factors of the nucleon. A basic reference model, the GKex model of Lomon, has been assumed; since it is very successful in representing the Q^2 dependence of the published high-quality data available to date. This approach is based on Vector Meson Dominance (VMD) together with coupling to the continuum which yields widths for the vector mesons and with asymptotics devised in such a way that the high- Q^2 behavior of pQCD is attained for very high momentum transfers — just how high is determined by the fit made to the data. No attempt has been made to refit the model to the most recent experimental results. Rather the model is taken to be “frozen” in the form in which it was presented in 2005 and thus the excellent agreement with more recent data may be taken as a test of its predictive power. The model is summarized in some detail in Sect. II together

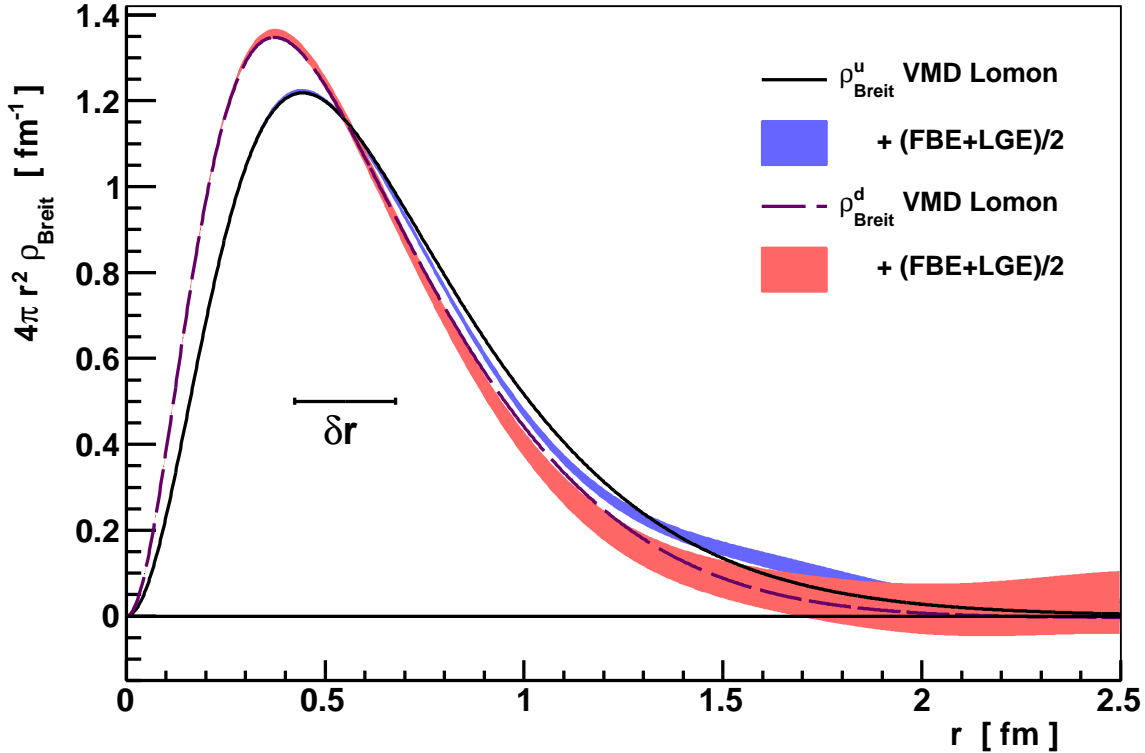


FIG. 22: Up and down quark coordinate-space Breit-frame electric distributions obtained using Eqs. (48) and (49). In color online.

with discussions of which specific data were fit and the fit results were presented in Sect. III.

In Sect. IV this reference model has been used to gain some insights into how the various contributions contained in it yield the observed behavior of the form factors. Specifically, it is shown in some detail how having a dipole form for a form factor is not natural in this approach, but rather arises from compensating effects where the more natural monopole form factors conspire effectively to yield roughly the dipole behaviors of the magnetic form factors at least at modest values of Q^2 . Such compensations do not occur for the electric form factor of the proton, in accord with the data where the ratio $G_E^p/[G_M^p/\mu_p]$ falls with Q^2 . All of the ingredients in the GKex model are displayed in some detail to ascertain which mesons are dominant and which are less important, at least for modest momentum transfers. Also, the effects arising from the inclusion of coupling to the continuum (in this model, only in the ρ meson contributions) are explored by comparing the form factors obtained with the width present or with only the ρ pole: these do not differ very significantly, indicating the

relatively minor role played by such effects.

Using the GKex model as a basis the differences between it and the data have been analyzed using sets of orthonormal functions to assess the level of uncertainty in the experimental results. In Sect. V both the data for the electric form factors with their uncertainties and the model for these quantities are Fourier transformed to coordinate space, obtaining the so-called Breit-frame distribution. It has been emphasized in the discussions in the body of the paper that, although these are well-defined mathematically, such Fourier transforms should not be interpreted as charge distributions. One might ask what use they are, given this statement. The point of view taken in the present study is that when one Fourier transforms both the data and the model form factors new insights into the roles played by the various mesons emerge. Specifically, it is clearly seen that at large distances (*i.e.* for large Breit-frame Fourier components) the ρ and the ω are dominant. As in momentum space, the width of the former may be turned on or off; the result is only a minor change, indicating that coupling to the continuum is not a major effect, at least for such Fourier components. In addition to obtaining the Breit-frame distributions as discussed above, in the same section the isoscalar/isovector and u-quark/d-quark distributions are also extracted for completeness.

The worldwide program over the last two decades to determine the elastic nucleon form factors using high duty factor electron accelerators to measure precisely polarization observables has been highly successful. It has yielded a data set of unprecedented precision and consistency for the nucleon elastic form factors at low and medium Q^2 . Although the BLAST low- Q^2 polarized data constitute a very small part of the whole data set, they have cast doubt on indications seen in earlier data of structure at this low momentum transfer. These were attributed to a “pion cloud”. Such structure is not present in the GKex representation, and indeed the coupling to explicit continuum pions is a relatively minor effect in this model, as discussed in the body of the paper. Further, very high quality measurements at low- Q^2 may help in reaching a definitive answer to the question of how much structure is actually present.

In this paper, we have used the vector meson dominance model and this new data set to understand the role of mesons in the electromagnetic form factors of the proton and neutron. Studies in both momentum space (for all four form factors) and in coordinate space (for the Breit-frame distributions that come from the nucleon’s electric form factors) have yielded

valuable insights. In a forthcoming paper, the study will be extended to include new data for the nucleon magnetic form factors and to investigate the corresponding coordinate space Breit-frame distributions.

Acknowledgments

This work has been supported by the United States Department of Energy under Cooperative Agreement DE-FC02-94ER40818 and the National Science Foundation Award No. PHY-0855584.

-
- [1] J. Bjorken and S. Drell, *Relativistic Quantum Mechanics* (McGraw-Hill, Inc, 1964).
 - [2] P. A. M. Guichon and M. Vanderhaeghen, Phys. Rev. Lett. **91**, 142303 (2003).
 - [3] P. G. Blunden, W. Melnitchouk, and J. A. Tjon, Phys. Rev. **C72**, 034612 (2005).
 - [4] C. E. Carlson and M. Vanderhaeghen, Ann. Rev. Nucl. Part. Sci. **57**, 171 (2007).
 - [5] T. W. Donnelly and A. S. Raskin, Annals Phys. **169**, 247 (1986).
 - [6] R. G. Arnold, C. E. Carlson, and F. Gross, Phys. Rev. **C23**, 363 (1981).
 - [7] W. Schroers et al. (LHPC) (2009), hep-lat/0910.3816.
 - [8] G. A. Miller, Phys. Rev. **C66**, 032201(R) (2002).
 - [9] H. H. Matevosyan, G. A. Miller, and A. W. Thomas, Phys. Rev. **C71**, 055204 (2005).
 - [10] H. H. Matevosyan, A. W. Thomas, and G. A. Miller, Phys. Rev. **C72**, 065204 (2005).
 - [11] G. A. Miller, E. Piassetzky, and G. Ron, Phys. Rev. Lett. **101**, 082002 (2008).
 - [12] G. A. Miller, Phys. Rev. Lett. **99**, 112001 (2007).
 - [13] G. A. Miller and J. Arrington, Phys. Rev. **C78**, 032201(R) (2008).
 - [14] G. A. Miller (2008), nucl-th/0802.2563.
 - [15] J. A. Rinehimer and G. A. Miller, Phys. Rev. **C80**, 015201 (2009).
 - [16] F. Iachello, A. D. Jackson, and A. Lande, Phys. Lett. **B43**, 191 (1973).
 - [17] G. Hohler et al., Nucl. Phys. **B114**, 505 (1976).
 - [18] M. Gari and W. Krumpelmann, Phys. Lett. **B173**, 10 (1986).
 - [19] Z. Dziembowski, H. Holtmann, A. Szczurek, and J. Speth, Annals Phys. **258**, 1 (1997).
 - [20] E. L. Lomon, Phys. Rev. **C64**, 035204 (2001).

- [21] E. L. Lomon, Phys. Rev. **C66**, 045501 (2002), nucl-th/0203081.
- [22] B. Pasquini and S. Boffi, Nucl. Phys. **A782**, 86 (2007).
- [23] E. L. Lomon (2006), nucl-th/0609020v2.
- [24] S. Galster et al., Nucl. Phys. **B32**, 221 (1971).
- [25] M. A. Belushkin, H. W. Hammer, and U.-G. Meissner, Phys. Rev. **C75**, 035202 (2007).
- [26] J. J. Sakurai, in *Fourth Coral Gables Conference on Symmetry Principles at High Energy*, edited by A. Perlmutter and B. Kurconoglu (W.H. Freeman & co., San Francisco, CA, 1967).
- [27] W. R. Frazer and J. R. Fulco, Phys. Rev. **117**, 1609 (1960).
- [28] R. Bijker and F. Iachello, Phys. Rev. **C69**, 068201 (2004).
- [29] P. Mergell, U. G. Meissner, and D. Drechsel, Nucl. Phys. **A596**, 367 (1996).
- [30] M. F. Gari and W. Kruempelmann, Phys. Lett. **B274**, 159 (1992, Erratum-
ibid.B282:483,1992.).
- [31] M. E. Christy et al. (E94110), Phys. Rev. **C70**, 015206 (2004).
- [32] I. A. Qattan et al., Phys. Rev. Lett. **94**, 142301 (2005).
- [33] S. Kopecky, P. Riehs, J. A. Harvey, and N. W. Hill, Phys. Rev. Lett. **74**, 2427 (1995).
- [34] Y. A. Aleksandrov, Phys. Part. Nucl. **30**, 29 (1999).
- [35] O. Gayou et al. (Jefferson Lab Hall A), Phys. Rev. Lett. **88**, 092301 (2002).
- [36] V. Punjabi et al., Phys. Rev. **C71**, 055202 (2005, Erratum-ibid.C71:069902,2005.).
- [37] G. Ron et al., Phys. Rev. Lett. **99**, 202002 (2007).
- [38] C. B. Crawford et al., Phys. Rev. Lett. **98**, 052301 (2007).
- [39] A. J. R. Puckett et al., Phys. Rev. Lett. **104**, 242301 (2010).
- [40] W. Bartel et al., Nucl. Phys. **B58**, 429 (1973).
- [41] A. Puckett, Ph.D. thesis, Massachusetts Institute of Technology (2010).
- [42] C. Berger, V. Burkert, G. Knop, B. Langenbeck, and K. Rith, Phys. Lett. **B35**, 87 (1971).
- [43] K. M. Hanson et al., Phys. Rev. **D8**, 753 (1973).
- [44] F. Borkowski, P. Peuser, G. G. Simon, V. H. Walther, and R. D. Wendling, Nucl. Phys. **B93**, 461 (1975).
- [45] P. E. Bosted et al., Phys. Rev. **C42**, 38 (1990).
- [46] A. F. Sill et al., Phys. Rev. **D48**, 29 (1993).
- [47] R. C. Walker, B. W. Filippone, J. Jourdan, R. Milner, R. McKeown, D. Potterveld, L. An-
divahis, R. Arnold, D. Benton, P. Bosted, et al., Phys. Rev. D **49**, 5671 (1994).

- [48] L. Andivahis et al., Phys. Rev. **D50**, 5491 (1994).
- [49] J. J. Murphy, Y. M. Shin, and D. M. Skopik, Phys. Rev. **C9**, 2125 (1974).
- [50] R. Madey et al. (E93-038), Phys. Rev. Lett. **91**, 122002 (2003).
- [51] G. Warren et al. (Jefferson Lab E93-026), Phys. Rev. Lett. **92**, 042301 (2004).
- [52] E. Geis et al. (BLAST), Phys. Rev. Lett. **101**, 042501 (2008).
- [53] B. Wojtsekhowski, private communication.
- [54] W. Bartel et al., Phys. Lett. **B30**, 285 (1969).
- [55] W. Bartel et al., Phys. Lett. **B39**, 407 (1972).
- [56] A. S. Esaulov et al., Sov. J. Nucl. Phys. **45**, 258 (1987).
- [57] A. Lung et al., Phys. Rev. Lett. **70**, 718 (1993).
- [58] P. Markowitz et al., Phys. Rev. **C48**, R5 (1993).
- [59] H. Anklin et al., Phys. Lett. **B336**, 313 (1994).
- [60] E. E. W. Bruins et al., Phys. Rev. Lett. **75**, 21 (1995).
- [61] H. Anklin et al., Phys. Lett. **B428**, 248 (1998).
- [62] H. Gao, Nucl. Instrum. Meth. **A402**, 277 (1998).
- [63] W. Xu et al., Phys. Rev. Lett. **85**, 2900 (2000).
- [64] G. Kubon et al., Phys. Lett. **B524**, 26 (2002).
- [65] B. Anderson et al. (Jefferson Lab E95-001), Phys. Rev. **C75**, 034003 (2007).
- [66] J. Lachniet et al. (CLAS), Phys. Rev. Lett. **102**, 192001 (2009).
- [67] C. E. Jones-Woodward et al., Phys. Rev. **C44**, R571 (1991).
- [68] T. Eden et al., Phys. Rev. **C50**, R1749 (1994).
- [69] I. Passchier et al., Phys. Rev. Lett. **82**, 4988 (1999).
- [70] D. Rohe et al., Phys. Rev. Lett. **83**, 4257 (1999).
- [71] J. Becker et al., Eur. Phys. J. **A6**, 329 (1999).
- [72] C. Herberg et al., Eur. Phys. J. **A5**, 131 (1999).
- [73] M. Ostrick et al., Phys. Rev. Lett. **83**, 276 (1999).
- [74] J. Golak, G. Ziemer, H. Kamada, H. Witala, and W. Glockle, Phys. Rev. **C63**, 034006 (2001).
- [75] H. Zhu et al. (E93026), Phys. Rev. Lett. **87**, 081801 (2001).
- [76] J. Friedrich and T. Walcher, Eur. Phys. J. **A17**, 607 (2003).
- [77] H. W. Hammer, D. Drechsel, and U.-G. Meissner, Phys. Lett. **B586**, 291 (2004).

- [78] G. P. Lepage and S. J. Brodsky, Phys. Rev. Lett. **43**, 545 (1979).
- [79] G. P. Lepage and S. J. Brodsky, Phys. Rev. **D22**, 2157 (1980).
- [80] N. Isgur and C. H. Llewellyn Smith, Phys. Rev. Lett. **52**, 1080 (1984).
- [81] N. Isgur and C. H. Llewellyn Smith, Nucl. Phys. **B317**, 526 (1989).
- [82] N. Isgur and C. H. Llewellyn Smith, Phys. Lett. **B217**, 535 (1989).
- [83] D. G. Crabb et al., Phys. Rev. Lett. **65**, 3241 (1990).
- [84] E. Tomasi-Gustafsson, F. Lacroix, C. Duterte, and G. I. Gakh, Eur. Phys. J. **A24**, 419 (2005).
- [85] S. Pacetti and E. Lomon, private communication.
- [86] N. Isgur, Phys. Rev. Lett. **83**, 272 (1999).
- [87] The DOE/NSF Nuclear Science Advisory Committee, *The Frontiers of Nuclear Science, A Long Range Plan* (2008), nucl-ex/0809.3137.
- [88] G. G. Simon, C. Schmitt, F. Borkowski, and V. H. Walther, Nucl. Phys. **A333**, 381 (1980).
- [89] L. E. Price et al., Phys. Rev. **D4**, 45 (1971).
- [90] T. Pospischil et al. (A1), Eur. Phys. J. **A12**, 125 (2001).
- [91] B. D. Milbrath et al. (Bates FPP), Phys. Rev. Lett. **80**, 452 (1998, Erratum-
ibid.82:2221,1999.).
- [92] S. Dieterich et al., Phys. Lett. **B500**, 47 (2001).
- [93] M. K. Jones et al. (Jefferson Lab Hall A), Phys. Rev. Lett. **84**, 1398 (2000).
- [94] J. J. Kelly, Phys. Rev. **C70**, 068202 (2004).
- [95] R. Madey et al., Eur. Phys. J. **A17**, 323 (2003).
- [96] M. Seimetz (A1), Nucl. Phys. **A755**, 253 (2005).
- [97] D. I. Glazier et al., Eur. Phys. J. **A24**, 101 (2005).
- [98] J. Bermuth et al., Phys. Lett. **B564**, 199 (2003).
- [99] J. J. Kelly, Phys. Rev. **C66**, 065203 (2002).
- [100] B. Pasquini and S. Boffi, Phys. Rev. **D76**, 074011 (2007).